The Effects of Pulsed Charging Current on the Performance and Lifetime of Lithium-Ion Batteries

Huang, Xinrong

DOI (link to publication from Publisher):
10.54337/aau456346192

Publication date:
2021

Document Version
Publisher's PDF, also known as Version of record

THE EFFECTS OF PULSED CHARGING CURRENT ON THE PERFORMANCE AND LIFETIME OF LITHIUM-ION BATTERIES

BY
XINRONG HUANG

DISSERTATION SUBMITTED 2021

AALBORG UNIVERSITY
DENMARK

The Effects of Pulsed Charging Current on the Performance and Lifetime of Lithium-Ion Batteries

Ph.D. Dissertation

Xinrong Huang

Dissertation submitted Sep., 2021

Dissertation submitted: Sep., 2021

PhD supervisor: Prof. Remus Teodorescu
Aalborg University, Denmark

Co-Supervisor: Assoc. Prof. Daniel-Ioan Stroe
Aalborg University, Denmark

PhD committee: Professor Søren Højgaard Jensen (chair)
Aalborg University

Professor Dr. Ir. Maitane Berecibar
Vrije Universiteit Brussel

Professor Torbjörn Thiringer
Chalmers University of Technology

PhD Series: Faculty of Engineering and Science, Aalborg University

Department: Department of Energy Technology

ISSN (online): 2446-1636
ISBN (online): 978-87-7210-080-7

Published by:
Aalborg University Press
Kroghstræde 3
DK – 9220 Aalborg Ø
Phone: +45 99407140
aauf@forlag.aau.dk
forlag.aau.dk

Printed in Denmark by Rosendahls, 2021

Abstract

The pulsed current charging has been proposed in the literature to improve the performance and maximize the lifetime of lithium-ion batteries by eliminating concentration polarization and improving the active material utilization. However, there are few studies on this charging technique, and some of them hold opposite opinions. Moreover, the effect of the pulsed current is inconclusive due to the changeable current profile and conditions. Therefore, the main objective of this work is to prove that the pulsed charging current under suitable conditions can improve the performance and extend the lifetime of lithium-ion batteries.

Various pulsed current charging modes and their effects on battery performance and lifetime are reviewed. Moreover, the main factor that impacts the battery performance and lifetime are analysis and discussed according to the previous studies.

The effects of pulsed current on the charging performance of batteries are experimentally investigated. The considered conditions include current modes, frequency, duty cycle, amplitude, and temperature. The main factors that impact the performance of batteries (i.e., obtained capacity, maximum rising temperature, and charging time) are analyzed and discussed. The results illustrate that the pulsed current has no significant effect on the improvement of the performance of batteries.

The effects of the pulsed current charging at a frequency range between 0.05 Hz and 2 kHz on battery lifetime are studied through aging tests. Compared to the traditional Constant Current (CC) charging, the pulsed current can extend the lifetime, where the PPC charging at 2 kHz can improve the lifetime up to 105.5%. Moreover, the impacts of pulsed current charging on the degradation mode of batteries are determined by a two-stage degradation model. The results of the Internal Resistance (IR) evolution and the changes in Incremental Capacity Analysis (ICA) curves are presented to comprehensively analyze the effect of the pulsed current on battery lifetime.

The scientific contribution of this work is summarized as follows: the pulsed current charging has no significant improvement in performance but can significantly extend the lifetime of lithium-ion batteries, by more than 100%.

Resumé

Den pulserende strømopladning er blevet foreslået i litteraturen for at forbedre ydeevnen og maksimere levetiden for lithium-ion-batterier ved at eliminere koncentrationspolarisering og forbedre udnyttelsen af aktivt materiale. Der er imidlertid få undersøgelser om denne opladningsteknik, og nogle af dem har modsatte meninger. Desuden er effekten af den pulserede strøm uklar på grund af den ændrede strømprofil og betingelser. Derfor er hovedformålet med dette arbejde at bevise, at den pulserende ladestrøm under passende forhold kan forbedre ydeevnen og forlænge lithium-ion-batteriers levetid.

Forskellige pulserende nuværende opladningsmetoder og deres virkninger på batteriets ydeevne og levetid gennemgås. Desuden er den vigtigste faktor, der påvirker batteriets ydeevne og levetid, analyse og diskuteret i henhold til de tidligere undersøgelser.

Effekterne af pulserende strøm på batteriets opladningsevne undersøges eksperimentelt. De betragtede forhold omfatter aktuelle tilstande, frekvens, driftscyklus, amplitude og temperatur. De vigtigste faktorer, der påvirker batteriets ydeevne (dvs. opnået kapacitet, maksimal stigende temperatur og ladetid) analyseres og diskuteres. Resultaterne illustrerer, at den pulserede strøm ikke har nogen signifikant effekt på forbedringen af batteriernes ydeevne.

Virkningerne af den pulserende strømopladning ved et frekvensområde mellem 0,05 Hz og 2 kHz på batteriets levetid undersøges gennem ældningstest. Sammenlignet med den traditionelle opladning med konstant strøm (CC) kan den pulserede strøm forlænge levetiden, hvor PPC -opladningen ved 2 kHz kan forbedre levetiden op til 105,5 %. Desuden bestemmes virkningerne af pulserende opladning af batteriernes nedbrydningstilstand af en to-trins nedbrydningsmodel. Resultaterne af Intern Resistance (IR) -udviklingen og ændringerne i inkrementel kapacitetsanalyse (ICA) kurver præsenteres for omfattende at analysere effekten af den pulserede strøm på batteriets levetid.

Det videnskabelige bidrag fra dette arbejde er opsummeret som følger: den pulserende strømopladning har ingen signifikant forbedring af ydeevnen, men kan forlænge lithium-ion-batteriers levetid betydeligt med mere end 100 %.

Preface

This Ph.D. thesis is a summary of the Ph.D. project "*The Effects of Pulsed Charging Current on the Performance and Lifetime of Lithium-Ion Batteries*". This Ph.D. project is mainly supported by the China Scholarship Council (CSC). I would like to thank the CSC, as well as the AAU Energy, Aalborg University, Denmark, who supported me for conference participation several times during my Ph.D. study.

First of all, I would like to express my sincere gratitude to my supervisor, Professor Remus Teodorescu, for his patient and professional guidance throughout my Ph.D. project. This Ph.D. thesis could not be finalized without his support. I would also like to thank my co-supervisor, Associate Professor Daniel-Ioan Stroe, for his consistent advice and encouragement. It has been a great experience to work under their supervision.

Special thanks go to Associate Professor Jinhao Meng, for his kindness and inspiring discussion during my Ph.D. study. Many thanks to Dr. Anirudh Budnar Acharya for his valuable suggestions and helps.

I am also grateful to Dr. Songda Wang, Dr. Yuanyuan Li, Dr. Zhongting Tang, Dr. Qiao Peng, and all my lovely colleagues at the AAU Energy, Aalborg University for their help. Thanks to Ms. Yuying Xie, Mr. Jiacheng Sun, Mr. Kuangpu Liu, Ms. Xinyi Chen, Ms. Xiaoxi Yun, Ms. Qi Qin, Ms. Yufei Jiang, Ms. Luona Xu, and all my friends who are always believing in me.

Finally, I would like to express my sincere gratitude to my parents and my fiance Wenjie Liu for their endless love all the way. Your encouragement and support gave me the motivation for life and work.

Xinrong Huang
Aalborg University, September 27, 2021

Contents

Report

Chapter 1

Introduction

1.1 Background

The target of the Paris Agreement, settled in 2015, is to limit global warming by reducing greenhouse gas emissions [1]. In the transportation sector, Electric Vehicles (EVs) will gradually replace the traditional internal combustion engine to alleviate the environmental issues that result from the greenhouse gas emissions [2]. With the strong support worldwide, the annual sale of EVs has increased by around forty times in the last decade [3]. The global stock of EVs in 2020 hit the 10 million mark, accounting for 1% of the stock share. Fig. 1.1 shows the development in EV markets from 2010 to 2020, where China, United States, and Europe are the main regions that dominate the EV market [4]. In 2018, the clean energy ministry launched the EV30@30 campaign, which set a collective goal of speeding up deployment and achieving a 30% share of EV sales among participating countries by 2030 [5]. The campaign supports the EV market, including electric passenger cars, light commercial trucks, buses, and trucks. It is also committed to deploying charging infrastructure to provide sufficient power for deployed vehicles. The annual sales of EVs will reach 44 million vehicles by 2030 under the EV30@30 scenario, as shown in Fig. 1.2 [6].

Generally, there are four types of batteries that are applied in EVs, i.e., lead-acid battery, Nickel-Cadmium (Ni-Cd) battery, Nickel-Metal Hydride (Ni-MH) battery, and lithium-ion battery [7, 8]. The cost of the lead-acid battery is lower than other types of batteries. However, the disadvantages of lead-acid batteries are the short lifetime and low energy density [7]. Moreover, lead-acid batteries require a cooldown period due to the high amounts of heat that were generated during the charging process. Thus, lead-acid batteries cannot use fast charging technology, which will result in high cell temperature and thereby reducing the battery lifetime [9]. The Ni-Cd batter-

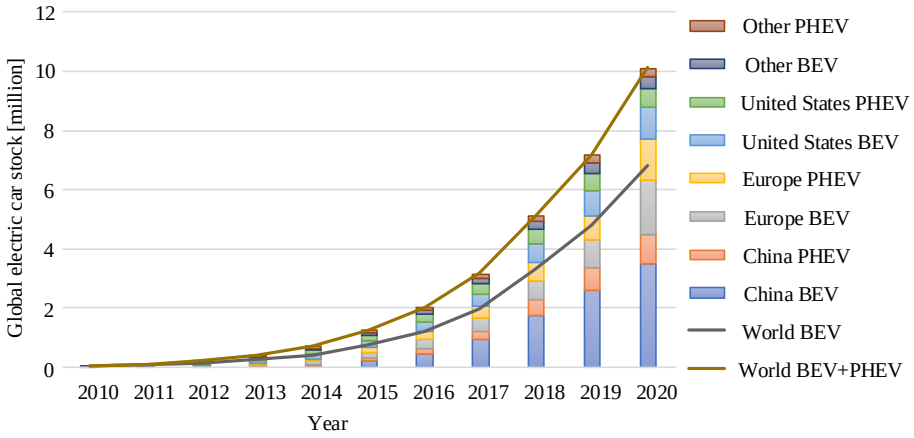

Fig. 1.1: Global electric passenger car stock, 2010-2020 [4]. (PHEV: plug-in hybrid electric vehicles; BEV: battery electric vehicles)

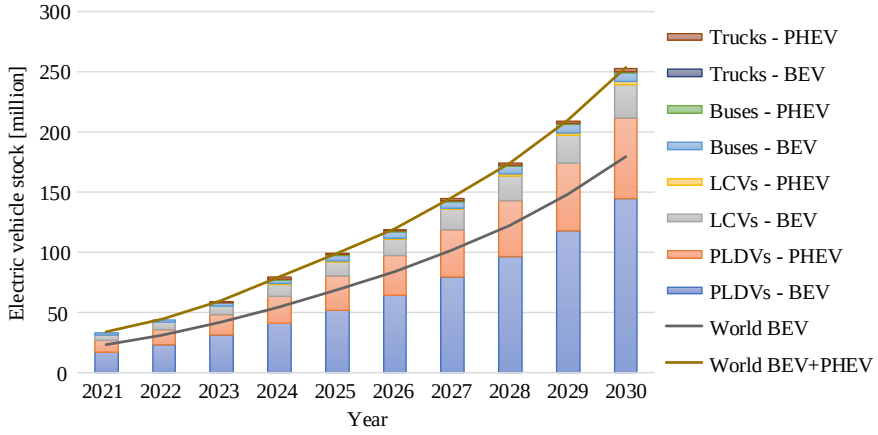

Fig. 1.2: Electric vehicle stock in the EV30@30 scenario, 2021-2030 [6]. (PLDV: passenger light duty vehicle, LCV: light commercial vehicle, BEV: battery electric vehicle, PHEV: plug-in hybrid electric vehicle.)

ies have some advantages, e.g., long lifetime and low cost, but suffer from low energy density as well as environmental issues [7]. Ni-MH batteries are environment-friendly and can be operated in a high voltage with desirable energy density. However, short cycle life is an issue for this type of batteries [10]. The lithium-ion battery techniques have been a popular choice for EV applications due to their high power and energy density, long lifetime, and low self-discharge rate [11]. Table 1.1 shows some specifications of the four types of batteries.

Table 1.1: Specifications of the Batteries in EVs [7, 12].

Battery type	Lead-acid	Nickel-Cadmium (Ni-Cd)	Nickel-Metal Hydride (Ni-MH)	Lithium-ion
Energy density [W/kg]	30-50	45-80	60-120	110-160
Cycle life	300-800	1500	300-500	500-2000
Self-discharge	Low	Moderate	High	Very low
Cost	Low	Average	Average	High
Nominal voltage [V]	2	1.25	1.25	3.6
Environmental issues	Moderate	High	Low	Low

However, the largest challenge that hinders the popularization of EVs is the high cost of lithium-ion batteries [13]. Several strategies have been adopted to reduce the cost of lithium-ion batteries, such as the exploration of lower-cost materials for lithium-ion chemistries, more cost-efficient battery manufacturing techniques, and mass-produced battery factories [14, 15]. Most of these methods are hard to implement shortly [16], while lifetime extension of lithium-ion batteries is a feasible solution to reduce the whole cost of EVs. The following section introduces several methods that can extend the lifetime of lithium-ion batteries.

1.1.1 Lifetime Extension of Lithium-ion Batteries

The lifetime extension is a huge challenge for the application of lithium-ion batteries. From the system level, developing advanced Battery Management Systems (BMSs) is necessary for EVs to ensure safe operation and extend the battery pack's service life. The main functions of the BMSs are monitoring and controlling the states of the cells in the battery pack. The optimal operating temperatures for lithium-ion batteries are between 15 °C and 35 °C [17]. Lower temperatures will lead to lithium plating and a loss of lithium inventory [18–20], while higher temperatures will result in rapid capacity fade due to the chemical side reactions such as the formation and growth of solid-electrolyte interface (SEI) [21]. Therefore, thermal management is an important part of BMSs to guarantee a safe and comfortable operating environment for batteries. To maintain the normal operating temperature, the cooling and heating systems are necessary for regulating environmental temperatures, which will increase the costs of EVs.

Balancing control is another method to extend the battery lifetime. The battery pack in EVs is assembled by tens or hundreds of battery cells connected in series and parallel. With the increase in the cycling number, the cells in the battery pack have different state-of-charge (SOC) and state-of-health (SOH), which can result in overcharging/overdischarging for some of the cells. Unbalanced states of the battery pack will accelerate the degrada-

tion and even lead to permanent damage of the battery cells [22]. To achieve the balance between cells, the simplest method is consuming the unbalancing energy by shunting resistors, which results in low energy efficiency. Various active balancing strategies are proposed, such as cell-to-cell, cell-to-pack, and pack-to-cell, which can transfer the energy from the high-energy cells to the low-energy cells [23–25]. In [26], an advanced balancing method based on the SOC and SOH is proposed, which can achieve the balance of the large battery pack with any number, aging states, and capacity deviation. However, the balancing control generally requires accurate SOC and SOH estimation.

Both the thermal management and balancing control extend the lifetime by controlling the operating states of the entire battery pack. At the cell level, developing an advanced charging strategy is essential to improve the charging performance and extend the battery lifetime [27]. The constant current (CC) charging is the most common-used charging strategy, which charges the battery cells by a specific current until the battery voltage reaches its maximum voltage. The CC charging is followed by the constant voltage (CV) phase to obtain a higher discharging capacity. During the CV phase, the current decreases until it reaches a predefined current value, e.g., 5% of 1 C current [28]. Therefore, the CC-CV charging strategy is a practical method to determine the battery capacity [29]. However, the CV phase increases the charging time by up to 48%, while it only contributes 22% of the discharging capacity [30]. Thus, the fast-charging stations recommend the users only charging the battery with the CC phase [31]. Various Multi-Stage Constant Current (MSCC) charging profiles have been proposed to optimize the charging performance and achieve different charging targets. In [32], a two-stage charging strategy is proposed to achieve 30-minute fast charging and improve the energy efficiency by 1% when compared with the CC charging strategy. In [33], a four-stage charging current profile based on Taguchi's method has been proposed to reduce the charging time. In [34], the Taguchi-based method is also applied to search the optimal MSCC pattern, which can improve the charging efficiency by 0.6–0.9% and lower cell's temperature by 2 °C when compared with the CC-CV charging. However, the MSCC charging requires accurate SOC estimation to switch the charging stage. Moreover, most of the MSCC charging methods are proposed to achieve fast charging and temperature control. Few of them further investigate the effect of the proposed MSCC charging on the lifetime of lithium-ion batteries. Therefore, even though the developing advanced charging strategy is a feasible way to extend the lifetime of batteries, no charging strategy has been widely proven to achieve this target so far.

1.1.2 Motivation

To extend the lifetime, it is necessary to develop advanced charging strategies for lithium-ion batteries by optimizing the charging current profiles. To avoid that the lifetime extension at the expense of the charging performance, such as the charging speed, the effects of the charging current on battery performance should be investigated at the same time. The pulsed current charging technique was previously proposed for Lead-acid batteries to extend their lifetime [35–38]. Then, it has been further applied in lithium-ion batteries to improve the charging performance and extend the lifetime [39–41]. As aforementioned, there are few studies on pulse current charging techniques, and some of them hold opposite opinions. For example, the authors in [41] claim that the pulsed current charging can extend the battery lifetime, while some other researchers reported that the pulsed current will result in a rapid capacity fade of the lithium-ion batteries [42]. Therefore, the effect of the pulsed current charging on the lifetime of lithium-ion batteries is not clear currently. Furthermore, the pulsed current is defined in different ways in the literature. In [41], the pulsed current can be represented as the constant current with periodic relaxation time. In [43], during the relaxation time, the current is not zero but a constant current that is lower than the positive current pulse. In [39], the pulsed current consists of a positive pulse, a negative pulse, and a relaxation time. In [44], the pulsed current is the positive current pulse followed by a negative current pulse. Moreover, the frequency of the pulsed current is a critical parameter, which can result in different effects on battery charging performance and lifetime [42, 45].

Even though the effect of the pulsed current on lithium-ion batteries has not been comprehensively presented in the literature, the pulsed current charging has been regarded as a promising charging strategy to improve the charging performance and lifetime of lithium-ion batteries [46–48]. Therefore, how the pulse current impacts the charging performance and lifetime of lithium-ion batteries needs to be further investigated.

1.2 Objectives and Limitations

1.2.1 Research question

This Ph.D. project aims to widen the knowledge of advanced charging strategies for lithium-ion batteries. The pulsed charging current has been previously proposed and studied; however, its effect on the performance and lifetime of lithium-ion battery cells is still inconclusive.

Therefore, the overall research question is defined as follows:

- **Can the pulsed charging current improve the performance and lifetime for lithium-ion batteries?**

1.2.2 Objectives

To answer this question, various pulsed current charging strategies need to be compared, and the effects of the pulsed current on charging performance and lifetime of lithium-ion batteries should be investigated. According to the overall research question, the main objective of this thesis is:

- **To prove that the pulsed charging current can improve the performance and extend the lifetime of lithium-ion batteries.**

In order to reach this main objective, three technical objectives are considered in this thesis, as follows:

- **Obj 1: Review of the pulsed current charging techniques for lithium-ion batteries.**

  Various pulsed current charging strategies will be reviewed in this thesis. According to the current profile, the fudamental current modes will be summarized and their definitions will be provided in detail. Moreover, the impacts of different pulse current modes on charging performance and lifetime will be reviewed. The main factor that impacts the performance and lifetime of lithium-ion batteries should be discussed according to previous studies.

- **Obj 2: Analyze the effects of the pulsed charging current on the performance of lithium-ion batteries.**

  The effects of the pulse current on the charging performance of lithium-ion batteries will be studied through experimental testing. Various test conditions of the pulsed current will be considered, such as the current modes, frequency, duty cycle, amplitude, and ambient temperature. According to the experimental results, the main factors that impact the battery capacity, maximum rising temperature, and charging time will be analyzed and discussed. The main factors that impact the charging performance of lithium-ion batteries will be obtained.

- **Obj 3: Analyze the effects of pulsed current charging on lifetime of lithium-ion batteries.**

  The frequency of the pulsed current is one of the critical parameters that influence the lifetime of lithium-ion batteries. The effects of the pulsed current charging on the lifetime of lithium-ion batteries will be investigated by aging tests considering a wide frequency range, i.e., between

0.05 Hz and 2 kHz. The optimal frequency for the lifetime extension of lithium-ion batteries will be obtained. By developing the degradation model, the impacts of pulsed current on battery degradation modes will be analyzed. Moreover, the evolutions in the internal resistance (IR) and incremental capacity analysis (ICA) curve will be presented to explore the effects of the pulsed current on the degradation of the batteries.

1.2.3 Limitations

There are several limitations in this Ph.D. project as follows:

- All experiments are performed using NMC-based battery cells with a nominal capacity of 2.2 Ah. The effects of pulsed charging current on lithium-ion battery cells with other chemical systems, e.g., LFP-based battery cells, which may show different results, are not investigated and discussed.
- Only the effects of the PPC on the lifetime of lithium-ion battery cells are investigated. Other pulsed current modes, e.g., the NPC and the APC, may result in different effects on the lifetime, which are not studied in this Ph.D. project.
- The different duty cycles of the pulsed current and different ambient temperatures that may result in different effects on the lifetime of lithium-ion battery cells are not investigated in this Ph.D. project.

1.3 Battery Cell Used in This Project

The type of battery used in this work is the lithium nickel cobalt oxide (NMC) cathode battery, which is the same battery technology for many of nowadays EVs, such as BMWi3 EVs [49]. The specifications of the tested battery cells are summarized in Table 1.2. Fig. 1.3 shows an NMC battery cell during the test in a climate chamber, which ensures a stable and reliable ambient temperature during all the measurements. The voltage, current, and temperature of battery cells are measured during all testing processes.

1.4 Thesis Outline

The outcomes of the Ph.D. project are summarized in this Ph.D. thesis, which includes a report and selected publications. The structure of the thesis is presented in Fig. 1.4. There are five chapters in the report, and the relevant

Table 1.2: Specifications of the tested battery cells.

Main parameter	Value
Model	HTCNR18650
Format	Cylindrical cell
Chemical system	NMC
Nominal capacity, Cap_n	2,200 mAh
Nominal voltage, V_n	3.6 V
Maximum voltage, V_{max}	4.2 V
Minimum voltage, V_{min}	2.5 V
Maximum (dis)charging current, I_{max}	3 C (6.6 A)

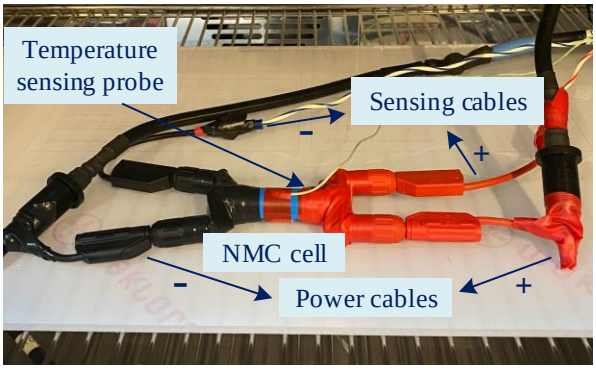

Fig. 1.3: A battery cell is under test in a climatic chamber.

papers are mentioned in the corresponding chapters. The objectives **Obj 1 - Obj 3** are discussed in *Chapters 2-4*, respectively.

Chapter 1 is the introduction of the thesis and presents the background, motivation, objectives, and limitations of this project.

Chapter 2 reviews the pulsed current charging techniques for lithium-ion batteries, including five pulsed current charging strategies, four negative pulsed current charging strategies, and a sinusoidal-Ripple current charging strategy. Several basic pulsed current modes are summarized and their definitions are described in detail. Furthermore, the effects of various pulsed current charging strategies on performance and lifetime are reviewed. Furthermore, the main factors that impact the performance and lifetime of lithium-ion batteries are summarized.

Chapter 3 is dedicated to investigating the effects of the pulsed current on the charging performance of the lithium-ion batteries. The investigated

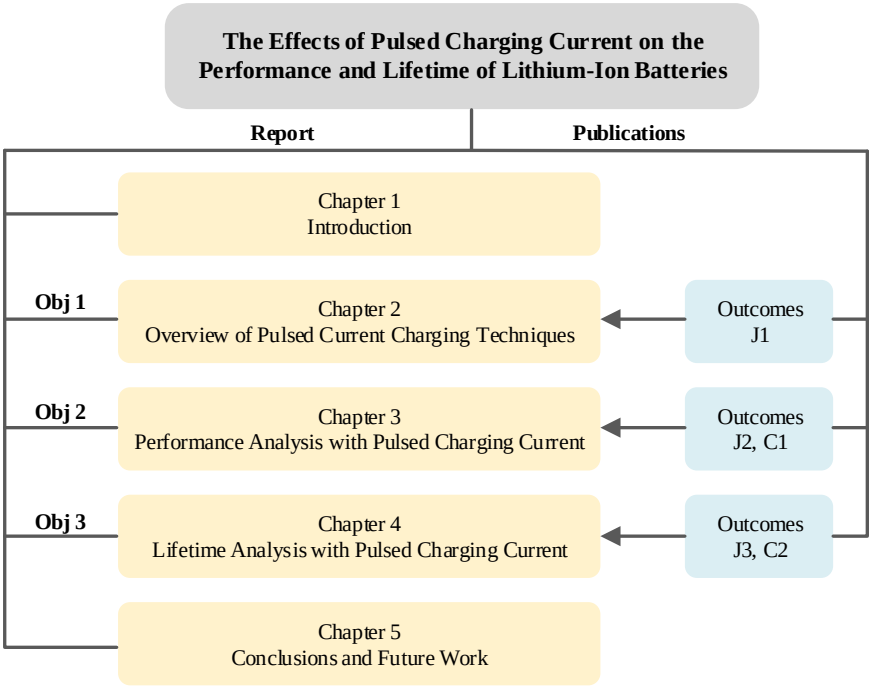

Fig. 1.4: Thesis structure and related publications.

charging performance includes the battery capacity, maximum rising temperature, and charging time. The battery cells were charged by various test conditions regarding the current modes, frequencies, duty cycles, amplitude, and ambient temperature. The factors that impact the charging performance are analyzed and discussed based on experimental results.

Chapter 4 studies the aging effect of the pulsed current charging within a wide frequency range, i.e., from 0.05 Hz to 2 kHz, for lithium-ion battery cells. The experimental results illustrate that the pulsed current charging can improve the battery lifetime. Moreover, frequency is an important factor that influences the battery lifetime. A two-stage degradation model is developed to determine the effects of the pulsed current charging on degradation modes at different aging stages. Moreover, the impacts of pulsed current charging on degradation modes of batteries are explored by analyzing the capacity fade, IR evolution, and ICA curves.

Chapter 5 gives the conclusions and main contributions of this project. Finally, the future research perspectives are presented.

1.5 List of Publications

The research dissemination during the Ph.D. project is shown below in the form of journal papers and conference publications. Parts of them are used in the Ph.D. thesis, i.e., J1, J2, J3, C1, and C2.

Journal Papers

J1. **X. Huang**, Y. Li, A. B. Acharya, X. Sui, J. Meng, R. Teodorescu, and D. I. Stroe, "A Review of Pulsed Current Technique for Lithium-ion Batteries" *Energies*, vol. 13, no. 10, p. 2458, May. 2020.

J2. **X. Huang**, W. Liu, A. B. Acharya, J. Meng, R. Teodorescu, and D. I. Stroe, "Effect of Pulsed Current on Charging Performance of Lithium-ion Batteries" *IEEE Trans. Ind. Electron.*, under review, 2021.

J3. **X. Huang**, W. Liu, J. Meng, Y. Li, S. Jin, R. Teodorescu, and D. I. Stroe, "Lifetime Extension of Lithium-ion Batteries with Low-Frequency Pulsed Current Charging" *IEEE J. Emerg. Sel. Topics Power Electron.*, under review, 2021.

Conference Papers

C1. **X. Huang**, Y. Li, J. Meng, X. Sui, R. Teodorescu, and D. I. Stroe, "The Effect of Pulsed Current on the Performance of Lithium-ion Batteries" in *Proc. IEEE ECCE*, pp. 5633-5640, Oct. 2020.

C2. **X. Huang**, S. Jin, J. Meng, R. Teodorescu, and D. I. Stroe, "The Effect of Pulsed Current on the Lifetime of Lithium-ion Batteries" in *Proc. IEEE ECCE*, accepted, 2021.

Other Publications which are not included in the thesis:

J4. X. Sui, D. I. Stroe, S. He, **X. Huang**, J. Meng, and R. Teodorescu, "The Effect of Voltage Dataset Selection on the Accuracy of Entropy-Based Capacity Estimation Methods for Lithium-Ion Batteries" *Applied Sciences*, vol. 9, no. 19, p. 4170, oct. 2019.

J5. J. Meng, L. Cai, D. I. Stroe, **X. Huang**, J. Peng, T. Liu, and R. Teodorescu, "An Automatic Weak Learner Formulation for Lithium-ion Battery State of Health Estimation" *IEEE Trans. Ind. Electron.*, in press, 2021.

C3. **X. Huang**, X. Sui, D. I. Stroe, and R. Teodorescu, "A Review of Management Architectures and Balancing Strategies in Smart Batteries" in *Proc. IEEE IECON*, pp. 5909-5914, Dec. 2019.

C4. **X. Huang**, A. B. Acharya, D. I. Stroe, and R. Teodorescu, "A Pulse-Current Implementation Using Phase-Shift Modulation in Smart Battery" in *Proc. PCIM Europe*, pp. 1-6, Jul. 2020.

C5. **X. Huang**, A. B. Acharya, J. Meng, X. Sui, D. I. Stroe, and R. Teodorescu, "Wireless Smart Battery Management System for Electric Vehicles" in *Proc. IEEE ECCE*, pp. 5620-5625, Oct. 2020.

C6. X. Sui, S. He, J. Meng, D. I. Stroe, **X. Huang**, and R. Teodorescu, "Optimization of the discharge cut-off voltage in LiFePO4 battery packs" in *Proc. IEEE ECCE Europe*, pp. 1–8, Nov. 2019.

C7. X. Sui, S. He, D. I. Stroe, **X. Huang**, J. Meng, and R. Teodorescu, "A review of sliding mode observers based on equivalent circuit model for battery SoC estimation" in *Proc. IEEE ISIE*, pp. 1965-1970, Aug. 2019.

C8. X. Sui, S. He, **X. Huang**, R. Teodorescu, and D. I. Stroe, "Data smoothing in Fuzzy Entropy-based Battery State of Health Estimation" in *Proc. IEEE IECON*, pp. 1779-1784, Nov. 2020.

Chapter 2

Overview of Pulsed Current Charging Techniques

This chapter reviews various pulsed charging currents and their effects on the performance and lifetime of lithium-ion batteries. Moreover, the main factor that impacts the performance and lifetime are analyzed and discussed according to the existing studies. The related outcome is listed as follows:

J1. **X. Huang**, Y. Li, A. B. Acharya, X. Sui, J. Meng, R. Teodorescu, and D. I. Stroe, "A Review of Pulsed Current Technique for Lithium-ion Batteries" *Energies*, vol. 13, no. 10, p. 2458, May. 2020.

2.1 Introduction

According to the controlled input, the pulse charging technique can be categorized into voltage pulse charging and current pulse charging. For the voltage pulse charging, the required averaging current can be achieved by controlling the duty cycle and frequency of the switching device [50, 51]. Meanwhile, adaptive voltage pulse charging has been developed to reduce the charging time through searching the optimal frequency and duty cycle [52, 53]. To further improve the charging performance and lifetime of lithium-ion batteries, the pulsed current charging technology becomes a promising alternative [41, 54]. Moreover, the current pulse includes positive current pulse and negative current pulse [39, 41], which can be extended to derive various pulsed current modes [43, 44]. However, in literature, all the pulsed current modes are named pulsed current charging while showing different profiles. The effect of the pulsed current is inconclusive due to inconsistent evaluation criteria, e.g., definitions, evaluation methods, research targets, etc. [55, 56]. It is necessary to review all related studies on pulsed current charging techniques in order to provide guidance to develop advanced charging strategies and determine future research gaps [57].

This chapter reviews the pulsed current charging techniques. Various pulsed current charging modes are summarized and defined in Section 2.2. In Section 2.3, the

effects of the pulsed current on the performance and lifetime of lithium-ion batteries are summarized according to the previous work. Then, the main factor that influences the performance and lifetime of lithium-ion batteries is analyzed and discussed in Section 2.4. The summary is given in Section 2.5.

2.2 Pulsed Current Charging Mode

There are two kinds of the current pulse, i.e., positive pulse and negative pulse. Typical positive pulse modes are Positive Pulsed Current (PPC) mode and Pulsed Current-Constant Current (PCCC). For the negative pulse, the Negative Pulsed Current (NPC) mode and Alternating Pulse Current (APC) mode are basic current modes. According to the four fundamental current modes, some extended modes are proposed, e.g., Pulse Modulation (PM) mode, Constant Current-Pulsed Current (CC-PC) mode, Positive Pulsed Current-Constant Voltage (PPC-CV) mode, Negative Pulsed Current-Constant Voltage (NPC-CV) mode, and Multi-stage Negative Pulsed Current-Constant Voltage (MNPC-CV) mode. Moreover, Sinusoidal-Ripple Current (SRC) mode is also presented as it is often mentioned and investigated with the pulsed current together in literature. In the following, the definitions of those current modes are provided in detail.

2.2.1 Positive Pulsed Current

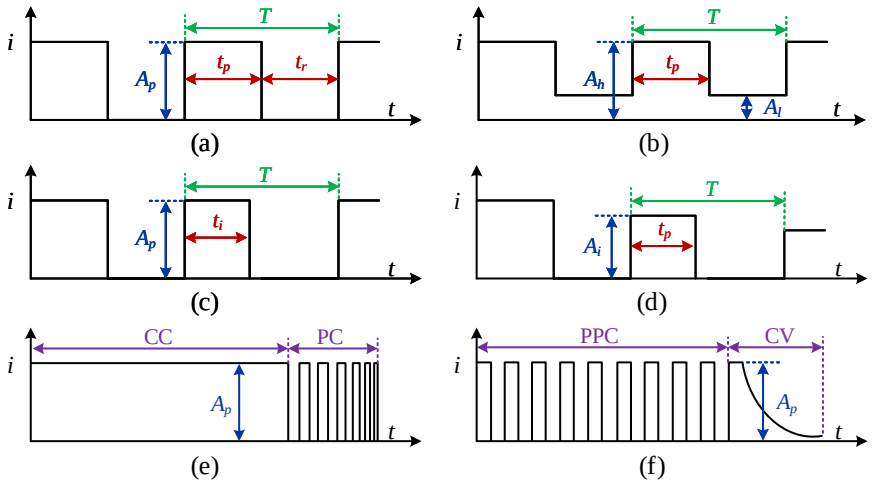

Fig. 2.1: (a) PPC mode, (b) PCCC mode, (c) PWM mode, (d) PAM mode, (e) CC-PC mode, and (f) PPC-CV mode.

1) PPC mode

The PPC mode is the constant current with the relaxation time, as shown in Fig. 2.1(a) [41]. The amplitude of the positive current pulse A_p is constant. The current is zero during the relaxation time. The frequency of the current pulse f is determined as follows:

$$f = \frac{1}{T} \tag{2.1}$$

where T is the pulse period. The duration of the current pulse is t_p, and the relaxation time is t_r. The duty cycle of current pulse, i.e., D_p, can be determined as follows:

$$T = t_p + t_r \tag{2.2}$$

$$D_p = \frac{t_p}{T}. \tag{2.3}$$

2) PCCC mode

The PCCC mode is a positive pulsed current followed by a constant current, as shown in Fig. 2.1(b) [43, 58, 59]. The amplitude of the constant current A_l is lower than that of the positive pulsed current A_h. The PCCC mode can be implemented by two current sources [60].

3) PM mode

To optimize the pulsed current mode, the PM mode was proposed and can be operated in two modes, i.e., Pulse Width Modulation (PWM) mode and Pulse Amplitude Modulation (PAM) mode [46, 61, 62]. In the PWM mode, the pulsed current amplitude A_p is constant, while the duration of pulse current t_i is variable, as shown in Fig. 2.1(c). On the contrary, in the PAM mode, the duration of the pulsed current t_p is constant, while the pulsed current amplitude A_i is variable, as shown in Fig. 2.1(d). The period T for both PWM and PAM modes is constant.

4) CC-PC mode

In the CC-PC mode, the battery cell is charged by a constant current A_P until the cell voltage reaches its maximum voltage V_{max}; then the battery cell is charged by the pulsed current, as shown in Fig. 2.1(e). The amplitude of the pulsed current is A_P and the average current of the pulsed current follows the CV profile, which is the same as the CV phase of the CC-CV mode [43, 63].

5) PPC-CV mode

The PPC-CV mode combines the PPC and CV modes, as shown in Fig. 2.1(f) [30, 64]. The period T, duty cycle D_p, and amplitude A_p of the current pulse in the PPC phase are constant. When the cell voltage reaches the maximum charging voltage, the charging process switches to the CV mode.

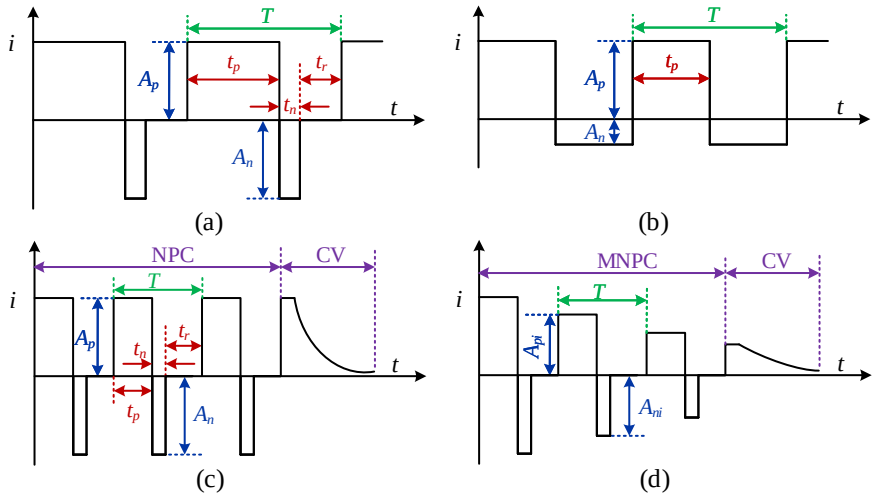

Fig. 2.2: (a) NPC mode, (b) APC mode, (c) NPC-CV mode, and (d) MNPC-CV mode.

2.2.2 Negative Pulsed Current

1) NPC mode

A period of the NPC mode consists of a positive current pulse, a negative current pulse, and a relaxation time, as shown in Fig. 2.2(a) [39, 65]. The period of NPC mode is T. The duration of the positive current pulse, negative current pulse, and relaxation are expressed as t_p, t_n, and t_r, respectively. The amplitude of the positive current pulse A_p and the negative current pulse A_n are constant values.

2) APC mode

The APC mode consists of the positive current pulse and the negative current pulse in a period, as shown in Fig. 2.2(b) [44, 46]. The amplitudes of the positive current pulse A_p and the negative current pulse A_n are constant.

3) NPC-CV mode

The NPC-CV mode combines the NPC and CV modes, as shown in Fig. 2.2(c) [40]. The battery cell is first charged by the NPC mode until the cell voltage reaches the maximum charging voltage. Then the battery cell is charged by the CV mode. The symbols of each variable of the NPC-CV mode are the same as in the NPC mode.

4) MNPC-CV mode

The MNPC-CV mode combines the MCC-CV and NPC-CV modes, as shown in Fig. 2.2(d) [45]. The amplitude of the positive current pulse $A_{p.i}$ and the negative current pulse $A_{n.i}$ is gradually decreased in the MNPC phase.

2.2.3 Sinusoidal-Ripple Current

The schematic of the Sinusoidal-Ripple Current (SRC) mode is presented in Fig. 2.3 [54]. The period of the current ripple is T. The amplitude and the offset of the current ripple are represented by A_{sr} and A_o, respectively. The amplitude of the SRC is the sum of A_{sr} and A_o.

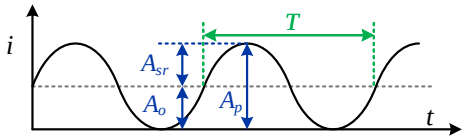

Fig. 2.3: Sinusoidal-Ripple Current (SRC) mode.

2.3 Effects of Pulsed Current on Battery Performance and Lifetime

The effects of positive pulsed current and negative pulsed current on the performance and lifetime of lithium-ion batteries are reviewed in this section. The relevant references and main results are summarized in tables.

2.3.1 Positive Pulsed Current

According to previous work, the frequency that returns the minimum impedance is regarded as the optimal frequency f_{Zmin}. The minimum impedance can be obtained by Electrochemical Impedance Spectroscopy (EIS) test. In [41], the PPC charging was considered under various conditions such as the frequency, duty cycle, and ambient temperature. According to the experimental results, the PPC charging under optimal conditions, i.e., f_{Zmin} (around 12 kHz), 50% duty cycle, and 23 °C ambient temperature, can increase the battery lifetime by 100 cycles when compared with the CC-CV charging. Moreover, the charging speed can be improved by 49% when compared with the CC-CV charging [66]. In [54], different frequencies were considered for the PPC charging. Compared with the CC-CV charging, the PPC charging at f_{Zmin} (i.e., around 1 kHz) can improve the discharging capacity by 2.1% and reduce the charging time by 16.8%, respectively. The obtained maximum rising temperature by the PPC charging at f_{Zmin} is lower than that of CC-CV charging, by 1.6 °C. However, in [30], the PPC-CV mode at f_{Zmin} (i.e., 2 kHz) has no significant effect on the charging speed and the capacity when compared with the CC-CV charging. Moreover, the PPC charging results in a higher maximum rising temperature when compared with the CC-CV charging [30]. In [67], the PPC charging has no effect on the charging speed but leads to a higher cell temperature when compared with the CC charging. In [42], the PPC-CV mode at 1 kHz has no significant impact on battery lifetime, while it can improve the charging speed by 17%. However, the PPC-CV at 50 Hz and 100

Hz results in faster degradation of the battery cell when compared with the CC-CV charging [42]. Therefore, it is inconclusive that the PPC mode at f_{Zmin} or other range of frequencies can improve the battery performance and lifetime.

In [64], the PPC-CV charging at 0.02 Hz has higher capacity retention when compared with the CC-CV charging. It needs to be noticed that the conclusion in [64] is obtained based on a pseudo-two-dimensional model instead of the practical tests. In [68], increasing the amplitude of the PPC charging from 0.5 C to 1 C can reduce the charging time by 82.8%; at the same time, it results in a decrease in charging capacity by 32.9% and an increase in cell temperature by 15.3 °C. When the duration of the positive pulse t_p increased from 1.2 s to 2 s, the charging time is shorted by 14.1%. Moreover, the rising temperature is not impacted by the relaxation time t_r. However, a long relaxation time enables the battery to discharge more capacity, by up to 20% [69].

In [43], the CC-PC charging and 25-Hz PCCC charging have an identical capacity fade rate like the CC-CV charging. The PCCC charging at 1 Hz shows a faster capacity fade when compared with the CC-CV charging [43]. The obtained capacity of the CC-PC and PCCC charging is 80%-95% of that by the CC-CV charging. The CC-PC charging results in a longer charging time due to the relaxation time during the PC phase. The PCCC does not impact the charging speed due to the same average current as that of the CC phase of the CC-CV charging.

The effects of positive pulsed current charging on the charging speed and charging/discharging capacity for lithium-ion batteries are summarized in Table 2.1. Table 2.2 is the maximum rising temperature that resulted from various frequencies. The effects of positive pulsed current charging on the lifetime of lithium-ion batteries are listed in Table 2.3.

Table 2.1: The effets of the positive pulsed current on the charging speed and charging/discharging capacity of lithium-ion batteries.

Ref.	Charging current	D_p	f	Compared to	Charging Speed	(Dis)charging Capacity
[66]	PPC	50%	f_{Zmin} (12 kHz)	CC-CV	+ 49%	-
[30]	PPC	50%	f_{Zmin} (2 kHz)	CC	Similar	+ 1.14%
	PPC-CV			CC-CV	Similar	+0.17%
[54]	PPC	50%	1 Hz	CC-CV	+ 16.2%	+ 1.3%
			100 Hz		+ 16.5%	+ 1.3%
			f_{Zmin} (around 1 kHz)		+ 16.8%	+ 0.6%
			10 kHz		+ 15.7%	+ 2.0%
[43]	PCCC	50%	1 Hz	CC-CV	Similar	Lower
	PCCC	50%	25 Hz		Similar	Lower
	CC-PC	-	-		Lower	Lower

Table 2.2: The effects of the positive pulsed current on the maximum rising temperature ΔT_{max} of lithium-ion batteries.

Ref.	Charging current	A_p	D_p	f	ΔT_{max}
[54]	PPC	1 C	50%	1 Hz	3.3 °C
				100 Hz	3.2 °C
				f_{Zmin} (around 1 kHz)	2.8 °C
				10 kHz	3.5 °C
[70]	PPC	0.5 C	50%	1 Hz	1.0 °C
				10 Hz	1.0 °C
				100 Hz	0.8 °C
				1 kHz	0.7 °C
				10 kHz	0.7 °C
				100 kHz	0.5 °C
[68]	PPC	1 C	29%	0.59 Hz	7.7 °C
			75%	0.50 Hz	8.0 °C
			80%	0.40 Hz	8.4 °C
			83%	0.56 Hz	8.7 °C
			68%	0.45 Hz	8.0 °C
			60%	0.40 Hz	7.7 °C
		2 C	75%	0.50 Hz	17.3 °C
		0.5 C	75%	0.50 Hz	2.0 °C

Table 2.3: The effects of the positive pulsed current on lifetime of lithium-ion batteries

Ref.	Charging current	D_p	f	Compared to	Impact on Lifetime
[41]	PPC	50%	f_{Zmin} (12 kHz)	CC-CV	+ 100 life cycles
[42]	PPC-CV	50%	1k Hz	CC-CV	-0.5%
			100 Hz		-12%
			50 Hz		-7.6%
[64]	PPC-CV	50%	0.02 Hz	CC-CV	+0.26%
[43]	PCCC	50%	1 Hz	CC-CV	Lower
	PCCC	50%	25 Hz		Similar
	CC-PC	-	-		Similar

2.3.2 Negative Pulsed Current

In NPC charging mode, the negative pulse and the relaxation time can improve the active material utilization rate and enable the battery cell to obtain a higher discharging capacity [39]. This means that the CV phase, which is used for obtaining a higher discharging capacity, can be removed, thereby reducing the charging time [39]. Moreover, the NPC charging can extend the lifetime by 128.6% when compared with the CC-CV charging [39]. The negative pulse can slow down the growth of the ohmic resistance and the charge transfer resistance during the aging process [39].

The NPC-CV charging with low amplitude and low frequency of the pulses can slow down the capacity fade of the battery cell [40, 45]. The cell temperature was not affected by the NPC charging due to the low frequency ($f < 0.1Hz$) and short duration of the negative pulse used in [40]. Various negative pulse amplitudes A_n and negative pulse time t_n were considered for NPC charging in [68]. Increasing the duration of the negative pulse can improve the battery capacity by around 3.3% when compared to the NPC charging with a short time of the negative pulse, while the charging time is prolonged by 36.9% due to the discharging current during the charging process. The rising temperature is not affected significantly by changing the duration of the negative pulse. Increasing the amplitude of the negative pulse will prolong the charging time and increase the rising temperature of the battery cell but has no significant effects on the charging capacity.

In [44], the charging performance is not affected by the APC charging, considering various frequencies, amplitudes, and duty cycles. In [70], it is observed that the APC charging at 10 kHz can reduce the capacity fade and decrease the rising temperature of the battery cell by around 6.5% and 25% when compared with that of 10 Hz. Even though these results indicate that the high frequency of the APC charging is better than that of the low frequency, no conclusion on how the APC mode affects battery cells is obtained since the APC mode is not compared to traditional CC/CC-CV mode in [70].

Table 2.4 presents the effects of negative pulsed current on the rising temperature of the lithium-ion batteries. The impacts of negative pulsed current on the lifetime of batteries are summarized in Table 2.5.

Table 2.4: The effects of the negative pulsed current on the maximum temperature rising ΔT_{max} of lithium-ion batteries.

Ref.	Charging current	A_P	A_n	t_n	ΔT_{max}
[40]	NPC-CV	1 C	0.5 C, 1C	1.3 s, 2.6 s, 5.1 s	1.0 °C
[68]	NPC	1 C	1 C	0.2 s	8.3 °C
			1 C	0.3 s	8.5 °C
			1 C	0.5 s	9.3 °C
			2 C	0.2 s	12.8 °C
			0.5 C	0.2 s	8.1 °C

Table 2.5: The effects of the negative pulsed current on the lifetime of lithium-ion batteries.

Ref.	Charging current	f	Compared to	Impact on Lifetime
[39]	NPC	×	CC-CV	+ 128.6%
[40]	NPC-CV	0.01 Hz	CC-CV	+0.2%
		0.005 Hz		+1.1%
[45]	NPC-CV	0.046 Hz, 0.023 Hz	CC-CV	+17.1%
	MNPC-CV	-		+14.4%

2.3.3 Sinusoidal-Ripple Current

In [54], the SRC charging can increase the charging speed and decrease the maximum rising temperature by 17% and 45.8%, respectively, when compared with the CC-CV charging. Moreover, the SRC at f_{min} can extend the battery lifetime by 16.1% when compared with the CC-CV charging. However, in [30] and [67], the SRC charging and CC charging show similar effects on battery charging speed and discharging capacity, while the rising temperature resulted from the SRC charging is higher than that of CC charging. Furthermore, the SRC charging has no significant impact on the capacity fade in the frequency range between 1 Hz and 1 kHz when compared with the CC charging [71].

Tables 2.6 - 2.8 summurize the effects of the SRC charging on battery performance and lifetime.

Table 2.6: The effects of the sinusoidal-ripple current on the charging speed and charging/discharging capacity of lithium-ion batteries.

Ref.	Charging current	f	Compared to	Charging Speed	(Dis)charging Capacity
[54]	SRC	1 Hz	CC-CV	+ 16.5%	+ 1.3%
		100 Hz		+ 16.7%	+ 1.3%
		f_{Zmin} (1 kHz)		+ 16.8%	+ 2.7%
		10 kHz		+ 16.0%	+ 1.3%
[30]	SRC	f_{Zmin} (2 kHz)	CC	Similar	+ 0.57%
	SRC-CV		CC-CV	Similar	-0.3%
[67]	SRC	228 Hz, 158 Hz	CC	Similar	Similar

Table 2.7: The effects of the sinusoidal-ripple current on the maximum temperature rising ΔT_{max} of lithium-ion batteries.

Ref.	Charging current	f	ΔT_{max}	Compared to CC/CC-CV
[54]	SRC	1 Hz	3.3 °C	-1.2 °C
		100 Hz	3.2 °C	-1.3 °C
		f_{Zmin} (1 kHz)	2.8 °C	-2 °C
		10 kHz	3.5 °C	-0.9 °C
[30]	SRC-CV	f_{Zmin} (2 kHz)	5.9 °C	+0.9 °C
[67]	SRC	228 Hz, 158 Hz	3.6 °C	+0.1 °C

Table 2.8: The effects of the sinusoidal-ripple current on lifetime of Lithium-ion batteries.

Ref.	Charging current	f	Compared to	Lifetime
[54]	SRC	f_{Zmin} (1 kHz)	CC-CV	16.1%
[71]	SRC	1 Hz, 100 Hz, 1 kHz	CC	Similar

2.4 Impact Factor

The pulsed current charging can be grouped into single-phase and two-phase charging, as shown in Figs. 2.1 and 2.2. The single-phase charging mode includes the PPC mode, PCCC mode, PWM mode, PAM mode, NPC mode, and APC mode (see Figs. 2.1(a)-(d) and Figs. 2.2(a)-(b)). The two-stage charging mode includes CC-PC mode, PC-CV mode, NPC-CV mode, and MNPC-CV mode (see Figs. 2.1(e)-(f) and Figs. 2.2(c)-(d)). When the average current is the same at the first phase, the second phase, usually a CV mode, enables the battery to spend more time obtaining a higher capacity. To investigate the main factor that impacts the battery performance and lifetime, the CV phase will not be considered in this section.

For the positive pulsed current, the main parameters are the frequency f, duty cycle D_p, relaxation time t_r, and amplitude A_p. For the negative pulsed current, the main parameters include the frequency f, negative pulse time t_n, relaxation time t_r, amplitude of negative pulse A_n. It is worth mentioning that the frequency of the negative pulse current usually occurs as the number of the negative pulse in the avaliable literature [40, 45]. For the sinusoidal-ripple current, the main parameters include the frequency f and amplitude A_p. Therefore, the main parameters can be concluded as the frequency, duty cycle, and amplitude for various pulsed charging currents. According to the available literature, this section analyzes the main parameters of pulsed current that impact the performance and lifetime of the lithium-ion batteries.

2.4.1 Impact Factor on Performance

In [66] and [54], the PPC charging and SRC charging can improve the charging speed of the lithium-ion batteries by removing the CV phase when compared with the CC-CV phase. If the CV phase is not considered for both pulsed current and constant current charging, the charging speed is not impacted by the current profile [67]. Moreover, the PPC charging and SRC charging can slightly improve the charging/discharging capacity (i.e., around 1.3%-2.7%) when compared with the constant current [54, 67].

In [68], the duration of both the positive pulse and negative pulse can impact the rising temperature (see Tables 2.2 and 2.4). A longer duration of the positive/negative pulse will result in a higher rising temperature. The increase in the negative pulse time results in a longer charging time because the battery is discharged periodically during the entire charging process. In contrast, the increase in the positive pulse time is equivalent to increase the average charging current, thereby reducing the charging time. The duration of the pulses can be equivalent to the duty cycle of the pulses according to Eq. 2.3. Therefore, the duty cycle is one of the factors that impact the rising temperature and the charging speed of the batteries.

Different frequencies of the pulsed current can result in different rising temperatures and charging/discharging capacities. However, the difference in these two performance within a large frequency range is not significant when other parameters, such as the amplitude A_p and the duty cycle D_p, are the same (see Tables 2.1, 2.2, 2.6, and 2.7) [54, 67, 70].

According to the discussion above, some conclusions can be obtained:

- The charging speed and the rising temperature are influenced by the duty cycle and the amplitude of the pulsed current. In fact, the duty cycle and the amplitude determine the average charging current, which is the main factor that impacts these two charging performances. A higher average charging current can reduce the charging time but increase the rising temperature of lithium-ion batteries.
- The charging/discharging capacity of the battery can be slightly improved by the pulsed current, but the impacts of the related parameters were rarely investigated in the literature.
- The frequency of the pulsed current has no significant impact on the investigated charging performance.

Furthermore, the existing studies have not compared various current modes and their impacts on battery performance.

2.4.2 Impact Factor on Lifetime

According to Tables 2.3, 2.5, and 2.8, frequency is an important factor that influences the battery lifetime, while other parameters of the pulsed current were rarely mentioned in previous work. Fig. 2.4 summarized the lifetime impacts resulted from various current modes and various frequencies in existing studies. Reference [39] also reported a significant lifetime extension by NPC charging when compared with the CC-CV charging. However, the frequency was not mentioned; thus it is not included

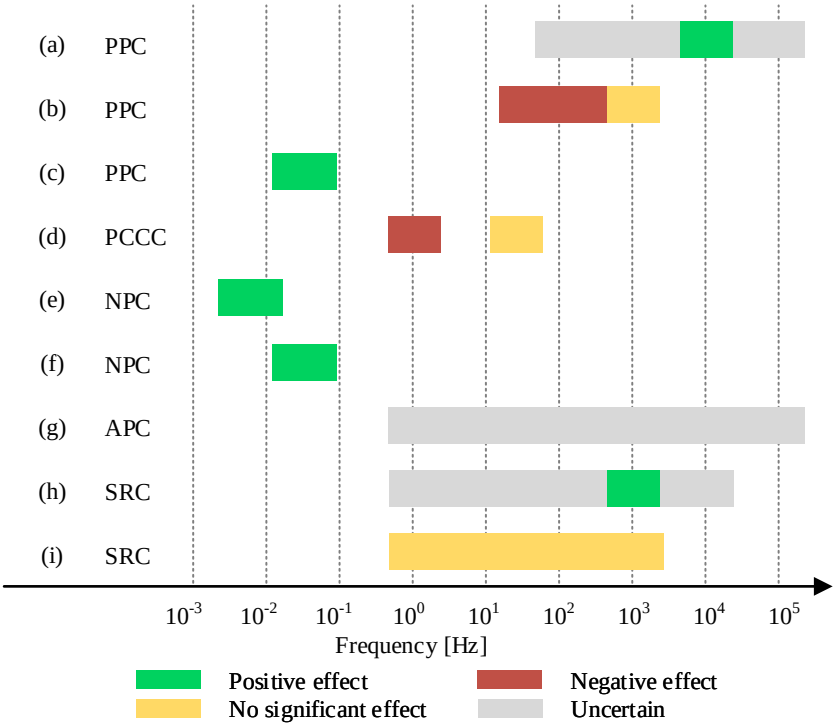

Fig. 2.4: Lifetime effect of pulsed current charging at different frequencies: (a) [41], (b) [42], (c) [64], (d) [43], (e) [40], (f) [45], (g) [70], (h) [54], and (i) [71].

in Fig. 2.4. Although different studies using different pulsed current modes, current parameters, and different evaluation methods, etc., some trends interrelated between the frequency and impact on battery lifetime can be observed:

- The frequency at the range between 1 Hz to 100 Hz has no effect and even negative effect on battery lifetime [42, 43, 71],
- The frequency that is lower than 1 Hz or is higher than 100 Hz has a positive effect on battery lifetime [40, 41, 45, 54, 64].

However, the optimal frequency range for the lifetime of the lithium-ion battery cells still needs to be investigated because no study has previously researched both high frequencies and low frequencies.

According to the current profile, there are five fundamental current modes, i.e., the PPC mode, PCCC mode, NPC mode, APC mode, and SRC mode, respectively. Table 2.9 summarizes the existing studies on the different current modes based on the experimental results. It can be observed that most of the previous works focused on the frequency and its effects on the charging performance and lifetime, while other parameters of the pulsed current, such as duty cycle and amplitude, were rarely mentioned.

2.5 Summary

This chapter reviewed and defined various pulsed current charging modes. According to the previous studies, the charging speed and the rising temperature are mainly affected by the duty cycle and the amplitude of the pulsed current, which can determine the average charging current. A higher average charging current can reduce the charging time but increase the rising temperature of lithium-ion batteries. The battery capacity can be slightly improved by the pulsed current, but the impacts of the related parameters, i.e., duty cycle and amplitude, were rarely mentioned in the literature. Moreover, the frequency of the pulsed current has no significant impact on the charging performance. However, the frequency of the pulsed current is one of the important factors that influence the battery lifetime. The pulsed charging current at low-frequency range (i.e., $f < 1Hz$) and high-frequency range (i.e., $f > 100Hz$) show a positive effect on performance in lifetime extension of lithium-ion batteries. In contrast, the pulsed charging current at the middle-frequency range (i.e., $1Hz < f < 100Hz$) has no positive effect on battery lifetime when compared with the traditional constant charging current. Several fundamental current modes, i.e., PPC mode, PCCC mode, NPC mode, APC mode, and SRC mode, and the relevant literature were summarized. The previous works mainly focused on the frequency and its effects on the performance and lifetime of batteries, while other parameters, such as duty cycle and amplitude, were few mentioned.

Table 2.9: The Existing studies on the pulsed charging current for lithium-ion batteries.

Reference	Chemical system	Current mode	Frequency [Hz]	Duty cycle [%]	Amplitude	Compared to	(Dis)charging capacity	Charging time	Rising temperature	Lifetime
[54]	NMC	PPC	1-10k	50	Constant	CC-CV	√	√	√	×
[30]	-	SRC PPC, PPC-CV, SRC, SRC-CV	2k	50	Constant	CC, CC-CV	√	√	√	√ ×
[41, 66]	LiPo	PPC	100-100k	20, 50, 80	Constant	CC-CV	×	×	×	√
[68]	NMC	PPC	0.45 - 0.59	29-83	0.5, 1 , 2	-	√	√	√	×
		NPC	-	-		-				
[42]	NMC	PPC-CV	50, 100, 1k	50	Constant	CC-CV	×	√	×	√
[43]	NMC, LCO, LFP	PCCC	1, 25	50	Constant	CC-CV	√	√	×	√
[39]	LCO	NPC	-	-	Constant	CC	×	×	×	√
[40]	LFP	NPC-CV	0.01, 0.005	-	0.5 C, 1 C	CC, CC-CV	×	×	×	√
[45]	LFP	NPC-CV	0.046, 0.023	-	Constant	CC-CV	×	×	×	√
[44]	LFP	APC	0.2-100	D_n: 1-10	0C-20C	CC-CV	√	×	×	×
[70]	LCO	APC	1-100k	50	Constant	-	×	×	√	√
[67]	NMC	SRC	158, 228		Constant	CC	×	√	√	×
[71]	NMC	SRC	1, 100, 1k	-	Constant	CC	×	×	×	√

√: studied; ×: not studied; -: not mentioned or uncertain
NMC: $LiNiMnCoO_2$
LiPo: Lithium-ion Polymer
LCO: $LiCoO_2$
LFP: $LiFePO_4$

Chapter 3

Performance Analysis with Pulsed Charging Current

This chapter focuses on the effects of pulsed charging current on the performance of lithium-ion batteries. The experimental tests will be performed with the pulsed charging current under various conditions, including current modes, frequencies, duty cycles, and amplitude. The related outcomes are listed as follows:

J2. **X. Huang**, W. Liu, A. B. Acharya, J. Meng, R. Teodorescu, and D. I. Stroe, "Effect of Pulsed Current on Charging Performance of Lithium-ion Batteries" *IEEE Trans. Ind. Electron.*, under review, 2021.

C1. **X. Huang**, Y. Li, J. Meng, X. Sui, R. Teodorescu, and D. I. Stroe, "The Effect of Pulsed Current on the Performance of Lithium-ion Batteries" in *Proc. IEEE ECCE*, pp. 5633-5640, Oct. 2020.

3.1 Introduction

The effects of various pulsed current modes on the performance of lithium-ion batteries have been studied to some extent in the available literature, which has been summarized in Table 2.9 of Chapter 2. However, the results of the related literature are inconclusive due to the difference in the lithium-ion battery chemistries. Moreover, there is no uniform standard for the evaluation of the pulse current in the existing studies. For example, the PPC charging can reduce the charging time by 16.6% when compared with the CC-CV charging [54], while the PPC charging has no significant impact on the charging time when compared with the CC charging [30]. Furthermore, only one or two pulsed current modes were investigated in each previous study, and considered frequency ranges of them are different. Therefore, it is necessary to compare various pulsed current modes with the uniform evaluation method. Most of the studies only investigated the frequency impacts, but the impact of the duty cycle and amplitude are not considered [57, 72]. Therefore, the impacts of the pulsed current with different parameters on battery performance should be further investigated.

This chapter investigates the effects of various pulsed current modes and pulsed current parameters on the performance of lithium-ion batteries. Section 3.2 introduces the considered performances, i.e., the maximum rising temperature, obtained capacity, and charging time/speed. The effects of six current modes on charging performances are investigated and compared in Section 3.3. In Section 3.4, the PPC charging with different duty cycles and amplitudes are considered to investigate the impacts of parameters on battery charging performance. The summary is given in Section 3.5.

3.2 Charging Performance

1) Maximum Rising Temperature

The maximum rising temperature is related to the safe operation and lifetime of the batteries. Therefore, the maximum rising temperature during the charging process is one of the important indicators to evaluate charging methods. The rising temperature of the battery cell mainly results from the overpotential heat Q_P [73], which is determined by Eq. (3.1):

$$Q_P = I_{rms}^2 R \tag{3.1}$$

where R is the resistance of the battery cell and I_{rms} is the RMS value of the current mode. The maximum rising temperature ΔT_{max} of the cell during the charging process can be obtained as follows:

$$\Delta T_{max} = T_{max} - T_{init} \tag{3.2}$$

where T_{init} and T_{max} are the initial and maximum temperatures of the battery cell, respectively.

2) Capacity

The obtained capacity is used to evaluate the charging capability of a charging method. The obtained battery capacity Cap can be calculated by the Coulomb counting method:

$$Cap = \frac{1}{3600} \int_0^t Idt \tag{3.3}$$

where I is the charging current. The improvement of the battery capacity ΔCap can be calculated by Eq. (3.4):

$$\Delta Cap[\%] = \frac{Cap - Cap_{CC}}{Cap_{CC}} \times 100\% \tag{3.4}$$

where Cap is the capacity obtained by the investigated pulsed charging current and Cap_{CC} is the capacity obtained by the CC.

3) Charging Time and Charging Speed

Charging time is one of the important indicators which is mainly determined by the current rate of the charging current. The charging speed α is the ratio between the obtained capacity Cap and the charging time t_{cha}:

$$\alpha = \frac{Cap}{t_{cha}} \tag{3.5}$$

A higher α value indicates a faster charging speed.

3.3 Performance Comparison of Pulsed Current Modes

This section investigates the effect of various current modes at a frequency range between 1 Hz and 1 kHz on the charging performance of an NMC-based battery cell. Moreover, the main factors that affect the charging performance are analyzed according to the experimental results. Finally, a comprehensive comparison of the considered current modes is performed.

3.3.1 Experimental Method

All experiments in this work were performed using a Kepco bidirectional programmable power supply, as shown in Fig. A.1 (see Appendix A.1). The tested battery cells were placed in a climatic chamber set at 25 °C.

The investigated current modes are presented in Fig. 3.1. The PPC mode, PCCC mode, NPC mode, APC mode, and SRC mode have been introduced in Section 2.2. In Fig. 3.1(f), the Alternating Sinusoidal-Ripple Current (ASRC) mode is the SRC mode with an additional dc offset, which enables that the battery is discharged periodically. The period of the current ripple is T. The amplitude and the offset of the current ripple are represented by A_{sr} and A_o, respectively. The CC mode is using for reference to evaluate these pulsed current modes.

For the CC mode, the RMS value of the current is the same as the current amplitude:

$$I_{rms.CC} = I_{CC} \tag{3.6}$$

The RMS value of each mode can be determined, as follows:

$$I_{rms.PPC} = \sqrt{D_p A_p^2} \tag{3.7}$$

$$I_{rms.PCCC} = \sqrt{D_p A_h^2 + (1 - D_p) A_l^2} \tag{3.8}$$

$$I_{rms.NPC} = I_{rms.APC} = \sqrt{D_p A_h^2 + D_n A_l^2} \tag{3.9}$$

$$I_{rms.SRC} = I_{rms.ASRC} = \sqrt{\frac{1}{2} A_{sr}^2 + A_o^2} \tag{3.10}$$

Therefore, different current modes and the corresponding parameters will result in the difference in I_{rms}.

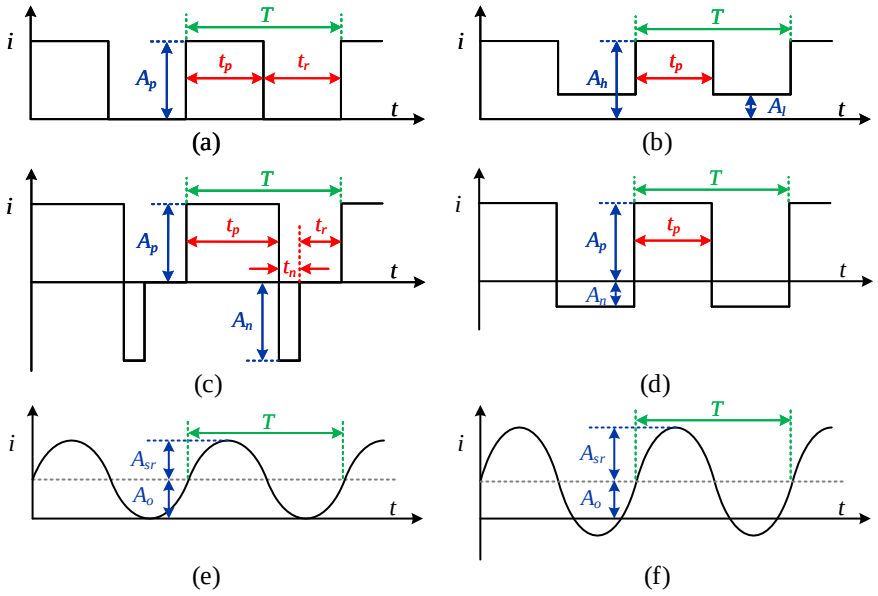

Fig. 3.1: Considered current modes: (a) PPC mode, (b) PCCC mode, (c) NPC mode, (d) APC mode, (e) SRC mode, and (f) ASRC mode.

Table 3.1: Main parameters of the current modes for ten cases.

Case	Current mode	Main parameters			
1	CC	1 C			
		$A_p(A_h)$ [C]	$D_p(D_h)$ [%]	$A_n(A_l)$ [C]	$D_n(D_l)$ [%]
2	PPC	2	50	-	-
3	PCCC	1.5	50	0.5	50
4	NPC	2	60	2	10
5	APC	2	75	2	25
6	APC	2.5	50	0.5	50
7	APC	3	50	1	50
		A_{sr} [C]		A_o [C]	
8	SRC	1		1	
9	ASRC	1.5		1	
10	ASRC	2		1	

Ten cases were considered, as shown in Table 3.1. Case 1 is the CC mode. Cases 2-4 are the PPC mode, PCCC mode, and NPC mode, respectively. Cases 5-7 are the APC mode with different amplitudes and duty cycles. Case 8 is the SRC mode. Cases

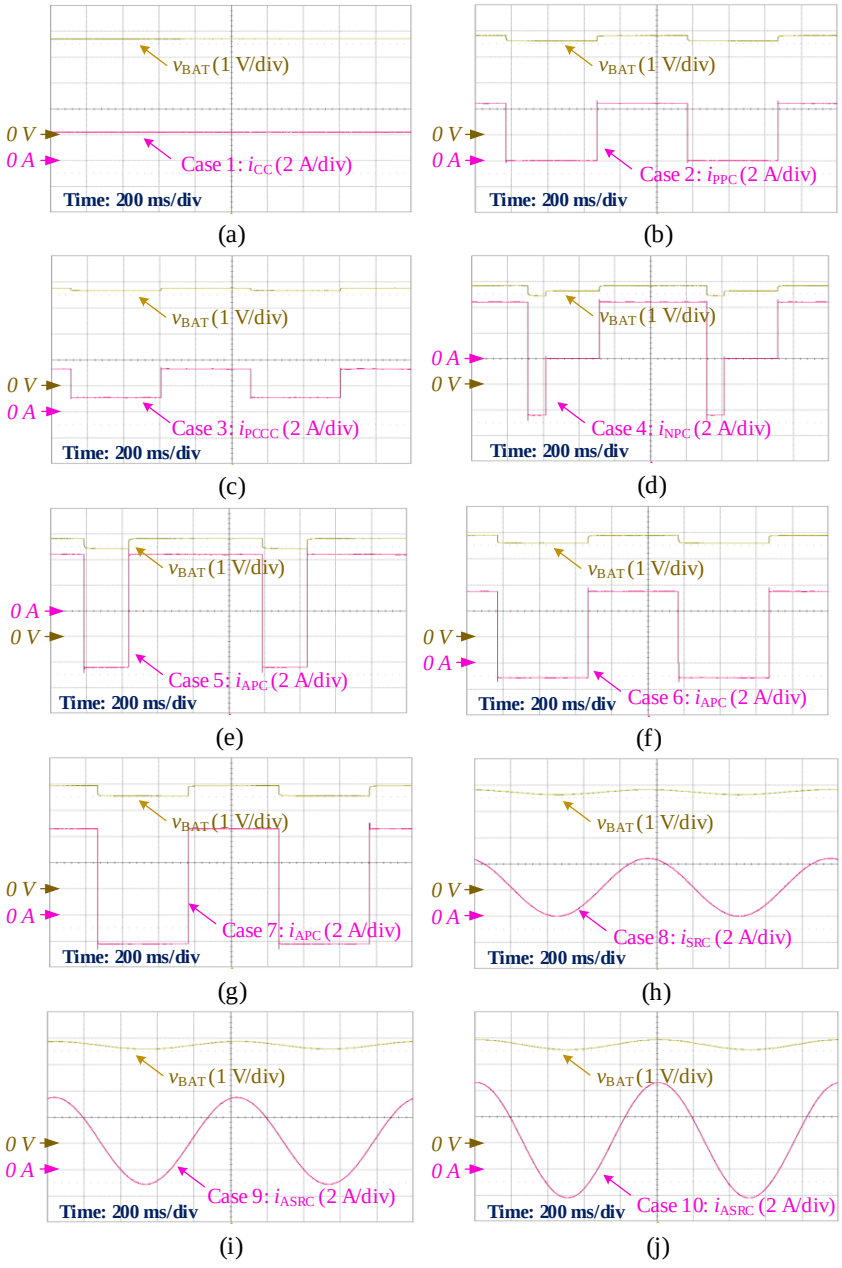

Fig. 3.2: The waveform of current modes during the tests: (a)-(j) correspond to Case 1-10. The frequency of Cases 2-10 is 1 Hz.

9-10 are the ASRC mode with different amplitudes. The investigated frequencies are 1 Hz, 10 Hz, 100 Hz, and 1 kHz. Fig. 3.2 shows the exemplification of each current mode of the ten cases, where the frequency of Cases 2-10 is 1 Hz. For each test case, the testing procedure presented in Fig. 3.3 was used.

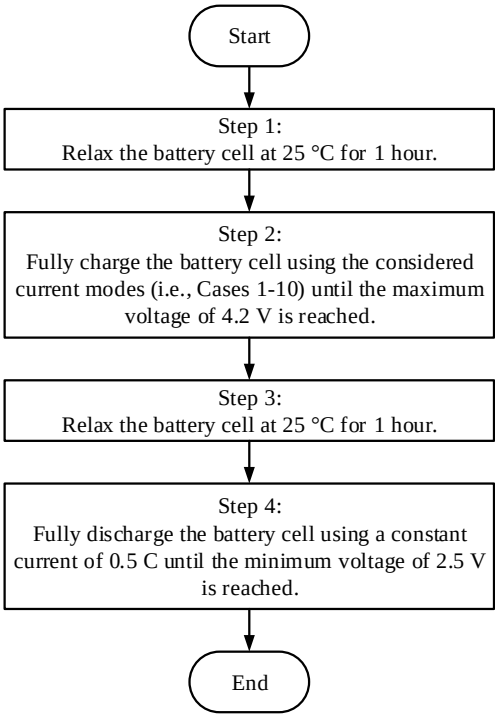

Fig. 3.3: Test procedures for each case.

3.3.2 Experimental Results

Tables 3.2-3.4 present the obtained results of the discharging capacity, charging time, and the maximum rising temperature, respectively, in which a darker color means a higher corresponding value. The CC mode, i.e., Case 1, is regarded as the reference to evaluate other cases. According to the results shown in Tables 3.2-3.4, the cell charged by the CC mode has the lowest capacity, the shortest charging time, and the lowest rising temperature.

In Table 3.2, for the four pulsed current modes at a frequency of 1 Hz, the discharging capacity obtained by NPC mode and APC mode is higher than that of PCCC mode and PPC mode. Moreover, the discharging capacity of the ASRC mode is higher than that of the SRC mode. Therefore, the discharging current during the charging process has a positive effect on the battery discharging capacity. Different conditions of the current modes can impact the discharging capacity, e.g., Cases 5-7. The charging time obtained by those current modes is different. However, comparing Table 3.2

Table 3.2: Discharging capacity of the tested cell under different test conditions.

Current mode		Cap_{dis} [mAh]			
Case 1	CC	1986			
frequency [Hz]		1	10	100	1k
Case 2	PPC	2027	2022	2019	2016
Case 3	PCCC	2006	2001	2000	1997
Case 4	NPC	2075	2072	2063	2060
Case 5	APC	2092	2090	2088	2085
Case 6	APC	2088	2087	2084	2077
Case 7	APC	2109	2106	2103	2100
Case 8	SRC	2023	2020	2017	2015
Case 9	ASRC	2033	2030	2026	2023
Case 10	ASRC	2084	2082	2078	2075

Table 3.3: Charging time of the tested cell under different test conditions.

Current mode		t_{cha} [s]			
Case 1	CC	3261			
frequency [Hz]		1	10	100	1k
Case 2	PPC	3273	3265	3260	3255
Case 3	PCCC	3290	3282	3280	3275
Case 4	NPC	3380	3375	3360	3356
Case 5	APC	3447	3443	3440	3435
Case 6	APC	3433	3430	3425	3415
Case 7	APC	3465	3460	3455	3450
Case 8	SRC	3280	3275	3270	3268
Case 9	ASRC	3326	3322	3315	3310
Case 10	ASRC	3425	3421	3415	3410

and Table 3.3, the charging time is proportional to the discharging capacity. In 3.4, the highest rising temperature is obtained by Case 7 conditions, which has the largest I_{rms}. In contrast, the lowest rising temperature is obtained by Case 1, which has the smallest I_{rms}. Table 3.5 presents the I_{rms} values of the ten cases, sorted from small to large. It can be observed that the rising temperature increases with the increase in the value of I_{rms}.

Frequency is another factor that impacts the charging performance of the battery

Table 3.4: Maximum rising temperature of the tested cell under different test conditions.

Current mode		ΔT_{max} [°C]			
Case 1	CC	2.8			
frequency [Hz]		1	10	100	1k
Case 2	PPC	3.4	3.4	3.4	3.3
Case 3	PCCC	3.0	2.8	2.8	2.7
Case 4	NPC	4.2	4.2	4.0	3.7
Case 5	APC	5.4	5.4	4.9	4.7
Case 6	APC	4.4	4.4	4.4	4.2
Case 7	APC	6.2	5.8	5.6	5.3
Case 8	SRC	3.1	3.0	3.0	2.9
Case 9	ASRC	3.6	3.5	3.5	3.4
Case 10	ASRC	4.3	4.3	4.3	4.0

cell. In Table 3.2, the current mode at a higher frequency obtains a lower discharging capacity compared to that of a lower frequency. Cases 2-9 at 1 Hz can averagely improve the discharging capacity by 0.5% when compared with that at 1 kHz, while the charging time of the former one is averagely longer than the later one by 0.5%. In 3.4, the maximum difference between the 1 Hz and 1 kHz is below 1 °C for each case. However, it can be observed that a lower frequency results in a higher cell temperature for each current mode.

In Eq. (3.1), two variables that impact the cell temperature are I_{rms} of the current mode and the resistance R of the battery cell. For each case, the value of I_{rms} is set to be constant according to Eqs. (3.6)-(3.10). Therefore, the battery resistance varies with the frequency and results in the different rising temperatures of the battery cell. To determine the resistance of the battery cell at different frequencies, the EIS test was performed using the Digatron battery test system to determine the battery impedance, where the real part of the impedance can be regarded as the resistance of the battery to analyze the heat generation. The measured battery ac-impedance between 6.5 kHz and 10 mHz is presented in Fig. 3.4. The real impedance $Z_{real}(f)$ of the battery cell increases as the frequency decreases in the predefined frequency range. Therefore, a lower frequency will result in a higher maximum rising temperature within the considered frequency range.

The form factor F is proposed to replace the RMS value I_{rms} to analyze the effect of vrious pulsed current modes on cell temperature without considering the real current value [44]. The form factor F is the ratio of the RMS value and the average current value of the current mode:

$$F = \frac{I_{rms}}{I_{avg}} \tag{3.11}$$

Fig. 3.5 shows the maximum rising temperature changes with the frequency f and form factor F. The form factor shows the dominant impact on the maximum rising

temperature of the battery cell when compared with the frequency. This is because the magnitude of the real part of the battery impedance $Z_{real}(f)$ is much smaller than that of the RMS value of the charging current I_{rms}.

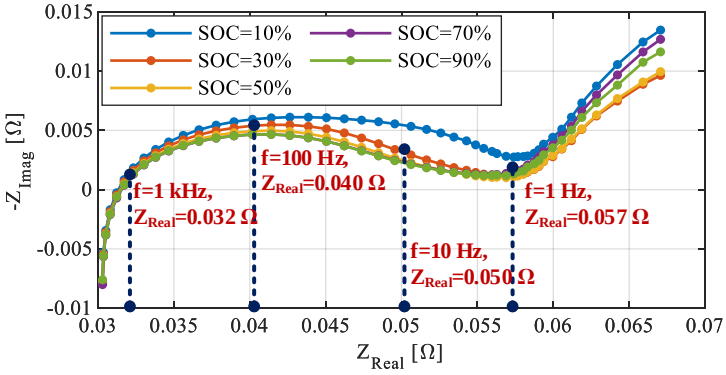

Fig. 3.4: The ac-impedance spectrum of the tested cell.

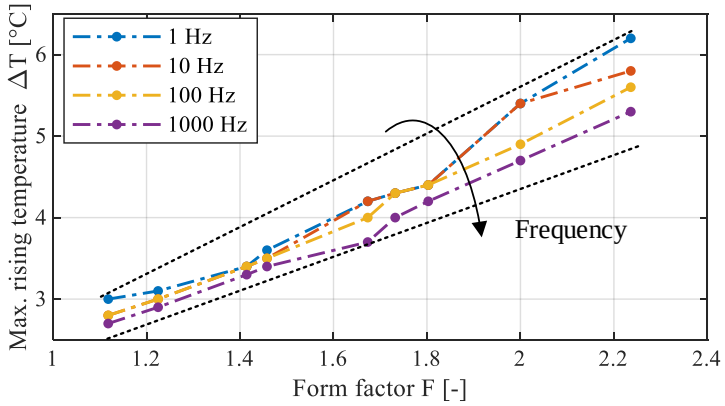

Fig. 3.5: The maximum rising temperature of the tested cell at different form factors and frequencies.

Table 3.5 summarizes experimental results obtained by ten cases. The frequency of Cases 2-10 is 1 Hz. The charging speed of PPC mode, i.e., Case 2, is higher than that of other cases. This is because the average current of Case 2 generated by the power supply is higher than that of other cases by around 0.01 A. Therefore, the charging speed is not affected by the current mode for lithium-ion battery cells.

The experimental results of the CC mode with 0.5 C are also presented in Table 3.5. As expected, the charging speed of the 0.5-C CC mode is slower than that of the 1-C CC mode by 50.1% due to the low average charging current. However, 0.5-C CC mode enables the battery cell to obtain a higher capacity by 6.9% and decrease the battery temperature by 1.6 °C compared to the 1-C CC mode. In APC mode, Case 7 enables the battery cell to obtain a higher capacity by 6.2%, close to the improvement effect of

0.5-CC mode but without slowing the charging speed. However, the maximum rising temperature of 0.5-C CC mode is lower than that of Case 7 by 5 °C.

Table 3.5: Experimental results of various cases when the frequency is 1 Hz.

Group	Current mode	I_{avg} [A]	I_{rms} [A]	t_{cha} [min]	Cap_{dis} [mAh]	ΔT_{max} [°C]	ΔCap [%]	α [mAh/min]
CC group	CC (0.5 C)	$0.5I_n$	$0.5I_n$	116.1	2124	1.2	6.9	18.3
	CC (Case 1)	I_n	I_n	54.4	1986	2.8	-	36.5
Positive-pulse group	PCCC (Case 3)	I_n	$\sqrt{1.25}I_n$	54.8	2006	3.0	1.0	36.6
	SRC (Case 8)	I_n	$\sqrt{1.5}I_n$	54.7	2023	3.1	1.9	37.0
	PPC (Case 2)	I_n	$\sqrt{2}I_n$	54.5	2027	3.4	2.1	37.2
Negative pulse group	ASRC (Case 9)	I_n	$\sqrt{2.125}I_n$	55.4	2052	3.6	3.3	36.7
	NPC (Case 4)	I_n	$\sqrt{2.8}I_n$	56.3	2075	4.2	4.5	36.8
	ASRC (Case 10)	I_n	$\sqrt{3}I_n$	57.1	2084	4.3	4.9	36.5
	APC (Case 6)	I_n	$\sqrt{3.25}I_n$	57.2	2088	4.4	5.1	36.5
	APC (Case 5)	I_n	$2I_n$	57.5	2092	5.4	5.3	36.4
	APC (Case 7)	I_n	$\sqrt{5}I_n$	57.8	2109	6.2	6.2	36.5

3.3.3 Discussion

To evaluate the investigated current modes, the results of the charging performance are scored by using the *normalize* function in MATLAB, as shown in Fig. 3.6. The charging speed is not affected by the current modes when their average current value are the same. Therefore, the charging speed is directly related to the average charging current instead of the current profile. The cell temperature during the charging process and the discharging capacity are affected by the current modes. The current modes can be divided into the positive-pulse group and the negative-pulse group. The current modes in the negative-pulse group include discharging current. The battery cell can obtain a higher capacity by the negative-pulse group when compared with the positive-pulse group. However, the negative-pulse group results in a higher maximum rising temperature compared with the CC mode. The rising temperature of the positive-pulse group is similar to that of the CC mode. Furthermore, the frequency does not show considerable effect on the performance of the battery cells during the charging process.

Even though some differences in the experimental results among various current modes can be observed, the overall charging performance of lithium-ion batteries has not been improved considerably. Moreover, the high rising temperature obtained by NPC and APC mode will be a challenge for EV applications, which consists of tens or even hundreds of battery cells to form a battery pack. Therefore, the pulsed current

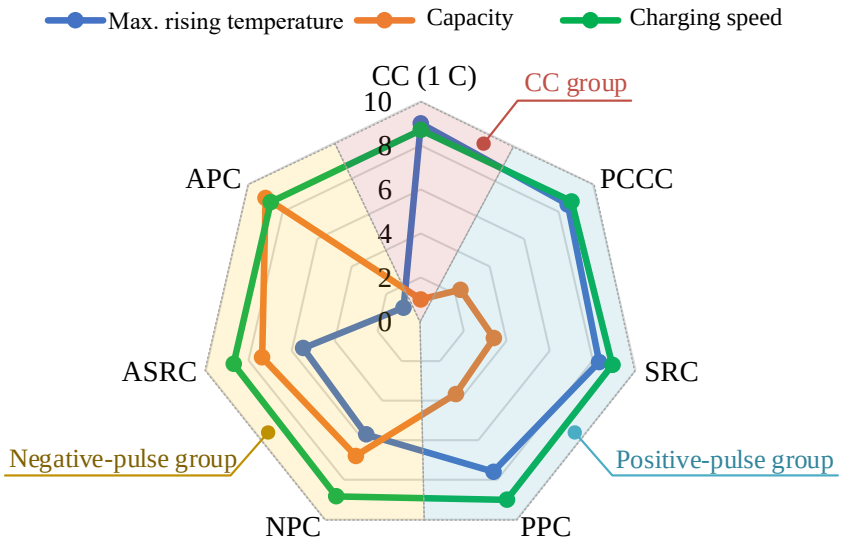

Fig. 3.6: Performance comparison of the investigated current modes.

charging has no considerable advantages in improving the charging performance of lithium-ion batteries.

3.4 Effect of PPC Parameters on Battery Performance

In the previous section, various current modes were evaluated using the CC mode at the same average current level. This section focuses on the impact of the different parameters of PPC mode on the charging performances of lithium-ion batteries. The CC mode with the same amplitude as the PPC mode is used as the reference to evaluate the influence of its parameters on the charging performance of the batteries.

3.4.1 Experimental Method

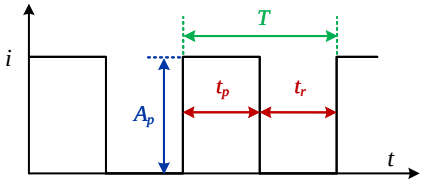

Fig. 3.7: Schematic of the Positive Pulsed Current (PPC) mode.

The experiments in this section were performed using the Digatron battery test system, as shown in Fig. A.2 (see Appendix A.2). The considered pulsed current mode is the PPC mode, as shown in Fig. 3.7.

The investigated parameters of the PPC are the duty cycle (i.e., 30%, 50%, 70%, and 90%) and the amplitude (i.e., 0.5 C, 1 C, 2C, 3C). Moreover, different ambient temperatures are also considered, i.e., 15 °C, 25 °C, 35 °C, 45 °C. The frequency of the pulsed current is 0.05 Hz in this work. The CC mode with the same amplitude as the PPC mode, i.e., $I_{CC} = A_p$, is regarded as the reference to evaluate the charging performance of the batteries. The test procedures used in this work are described as follows:

1. Temper the battery cell at 25 °C for 1 hour.
2. Fully discharge the battery cell using a 0.5 C current until the minimum voltage of 2.5 V is reached.
3. Relax the battery cell at 25 °C for 1 hour.
4. Fully charge the battery cell using a 0.5-C PPC mode with 30% duty cycle until the maximum voltage of 4.2 V is reached.
5. Relax the battery cell at 25 °C for 1 hour.
6. Fully discharge the battery cell using a 0.5-C PPC mode with 30% duty cycle until the minimum voltage of 2.5 V is reached.
7. Repete steps 3-6 for the different amplitudes: 1 C, 2 C, and 3 C.
8. Repete steps 3-7 for the different duty cycles: 50%, 70%, and 90%.
9. Repete steps 3-7 using the CC mode.
10. Repete steps 1-9 for the different ambient temperatures: 15 °C, 45 °C, and 35 °C.

3.4.2 Experimental Results

1) Capacity

The changes in the obtained battery capacity ΔCap is determined by Eq. (3.4). As several tests conditions were considered in this work, the ΔCap can be further defined as follows:

$$\Delta Cap_{T.C.D} = (\frac{Cap_{T.C.D}}{Cap_{T.C.100}} - 1) \times 100\% \tag{3.12}$$

where T and C are the ambient temperature and current rate of the amplitude, respectively; $Cap_{T.C.D}$ is the obtained capacity using the PPC with different duty cycles; $Cap_{T.C.100}$ is the capacity using a CC mode. The considered amplitude and the temperature conditions are the same for the PPC and CC modes.

The capacity changes caused by the pulsed current under different test conditions are presented in Fig. 3.8. When ΔCap is above the reference line, the obtained capacity using the PPC is higher than that of the CC mode. Some conclusions regarding the effects of the PPC on battery capacity are drawn according to the results:

- The duty cycle can considerably impact the battery capacity. For instancece, The PPC mode with a duty cycle of 30% can increase the capacity by 3.3% - 30.6% compared to the CC mode at the same current amplitude level.

- With the increase in duty cycles, the effects of the PPC mode on the capacity decreases. When the duty cycle is higher than 70%, the obtained capacity is lower than that of CC mode at 15 °C and 35 °C, independent of the current amplitude.
- With the ambient temperature increase, the capacity obtained by the PPC mode at the same duty cycle and amplitude conditions increases.
- When the ambient temperature is higher than 25 °C, the higher current amplitude further positively impacts the battery capacity when compared with the CC mode.

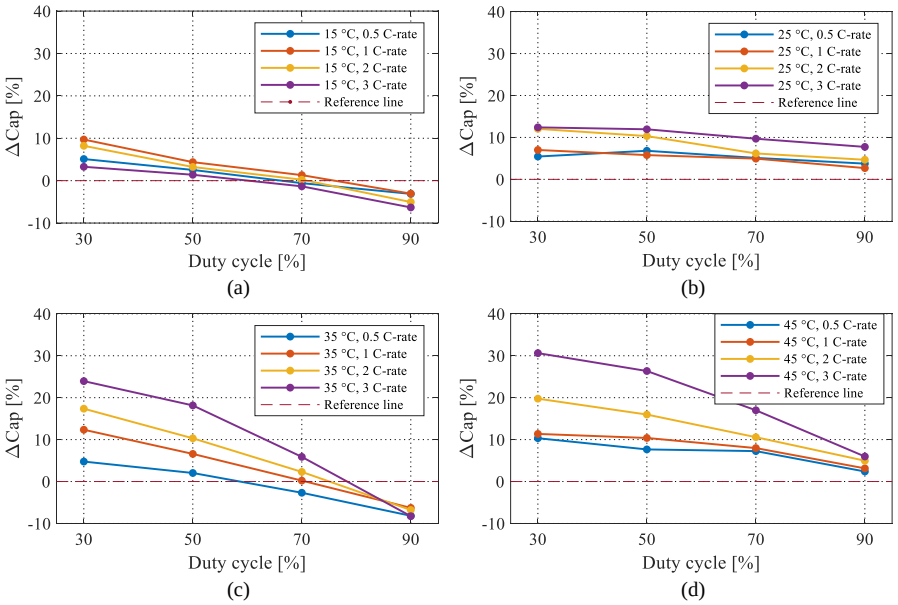

Fig. 3.8: The effects of the PPC with different amplitudes and duty cycles on the battery capacity: (a)-(d) correspond to 15 °C, 25 °C, 35 °C, and 45 °C, respectively.

2) Charging time

The ratio of the charging time t_{ratio} between the PPC mode and the CC mode is uded to analyze the effects of the PPC on the charging time, as follows:

$$t_{ratio} = \frac{t_{T.C.D}}{t_{T.C.100}} \tag{3.13}$$

where C and T are the current rate of the amplitude and the ambient temperature; $t_{T.C.D}$ is the charging time using the PPC with different duty cycles; $t_{T.C.100}$ is the charging time using a CC. The PPC and CC modes are compared under the same current amplitude and ambient temperature conditions. According to the results shown in Fig. 3.9, the charging time of the PPC is mainly impacted by the duty cycle. The lower duty cycle means the short duration of the pulse current during each period, thereby leading to a longer charging time.

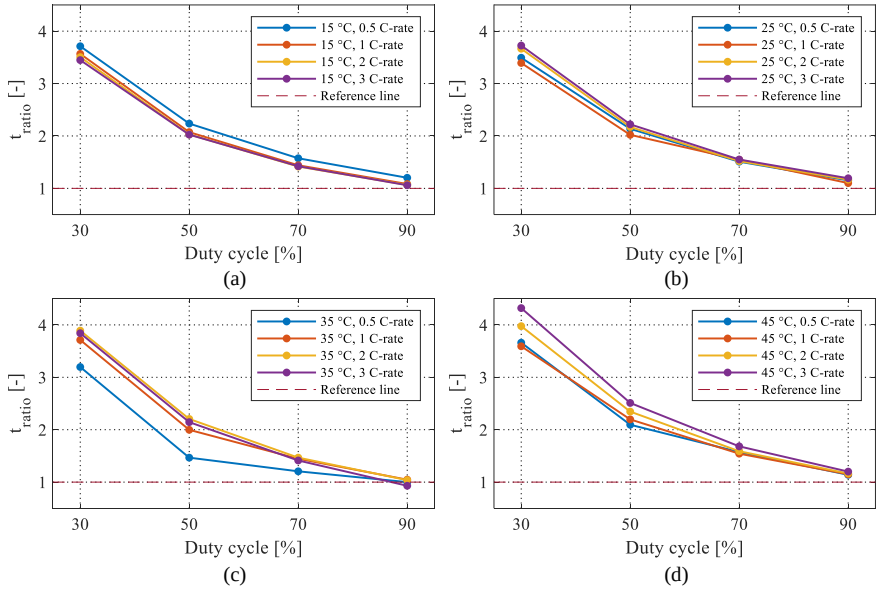

Fig. 3.9: The effect of the PPC with different amplitudes and duty cycles on the charging time of the battery: (a)-(d) correspond to 15 °C, 25 °C, 35 °C, and 45 °C, respectively.

3) Maximum rising temperature

The maximum rising temperature has been defined in Eq. 3.2. Considering various test conditions, it can be further expressed as follows:

$$\Delta T_{max.T.C.D} = T_{max.T.C.D} - T_{init.T.C.D} \tag{3.14}$$

where $T_{init.T.C.D}$, $T_{max.T.C.D}$, and $\Delta T_{max.T.C.D}$ are the initial temperature, maximum temperature, and the maximum rising temperatrue, respectively, under the corresponding test conditions. The results of the maximum rising temperature are presented in Fig. 3.10. The 100% duty cycle is represented the CC charging. As expected in Eq. (3.1), a higher current amplitude leads to a higher cell temperature. A lower duty cycle leads to a lower maximum rising temperature. Moreover, the changes in cell temperature at a low ambient temperature are larger than that at a higher ambient temperature.

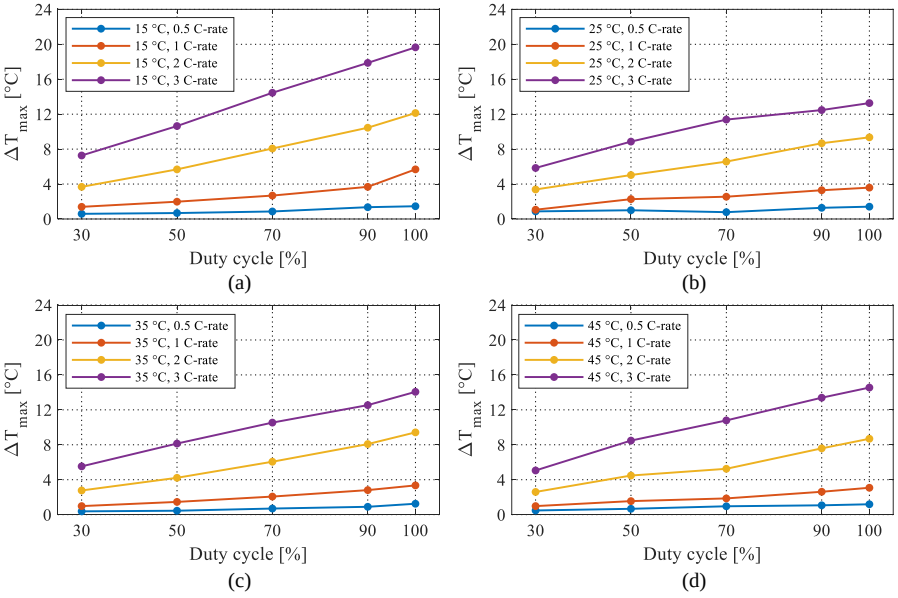

Fig. 3.10: The effect of the PPC with different amplitudes and duty cycles on the maximum rising temperature $\Delta T_{max.}$ of the battery: (a)-(d) correspond to 15 °C, 25 °C, 35 °C, and 45 °C, respectively.

4) Pulsed charging capacity modeling

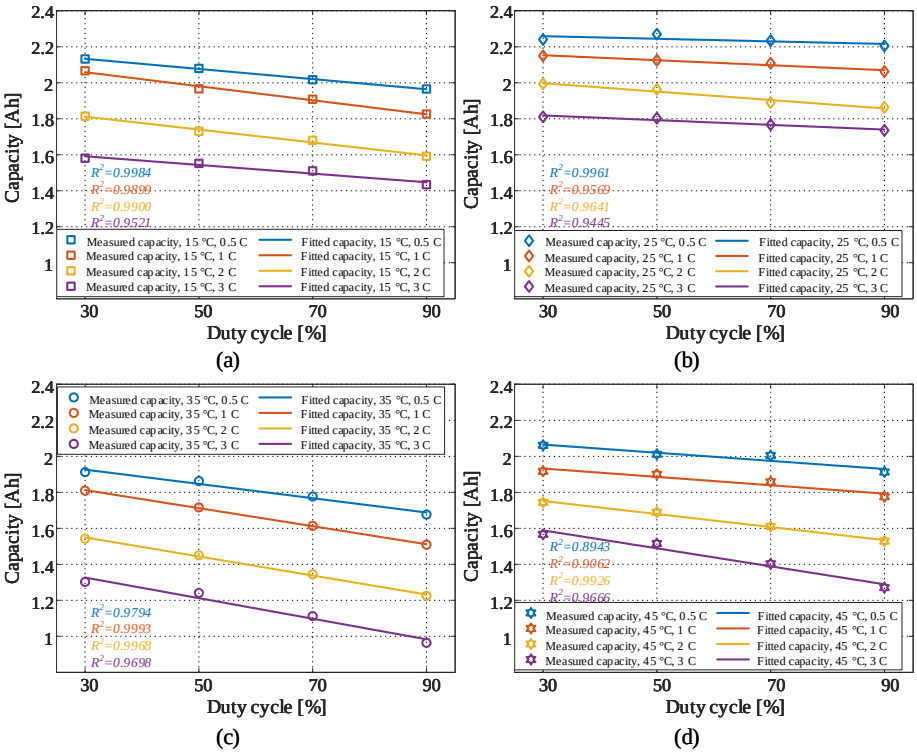

Fig. 3.11: Measured and fitted capacity of the battery cells with the PPC: (a)-(d) correspond to 15 °C, 25 °C, 35 °C, and 45 °C, respectively.

To parameterize the pulse charging capacity, a capacity model is developed using a function, which can fit the obtained capacity considering the duty cycles of the PPC (see the lines in Fig. 3.11). The measured capacities are the marked points in Fig. 3.11. The pulsed charging capacity can be expressed as a function of the duty cycle, temperature, and current amplitude as follows:

$$\begin{aligned} Cap(D,C,T) &= A_{1\times 2}(C,T)\cdot\begin{bmatrix} D \\ 1 \end{bmatrix} \\ &= \begin{bmatrix} A_1(C,T) & A_2(C,T) \end{bmatrix}\cdot\begin{bmatrix} D \\ 1 \end{bmatrix} \end{aligned} \tag{3.15}$$

where $A_{1\times 2}(C,T)$ represents the current rate of the amplitude and ambient temperature fitting coefficient. The accuracy of the fitting was quantified by the R^2 coefficient. To find a function that can describe the measured capacity, the dependence of $A_{1\times 2}(C,T)$ coefficient on the current rate of the amplitude should be explored as shown in Fig. 3.12. The relationship between $A_{1\times 2}(C,T)$ and the current rate can be

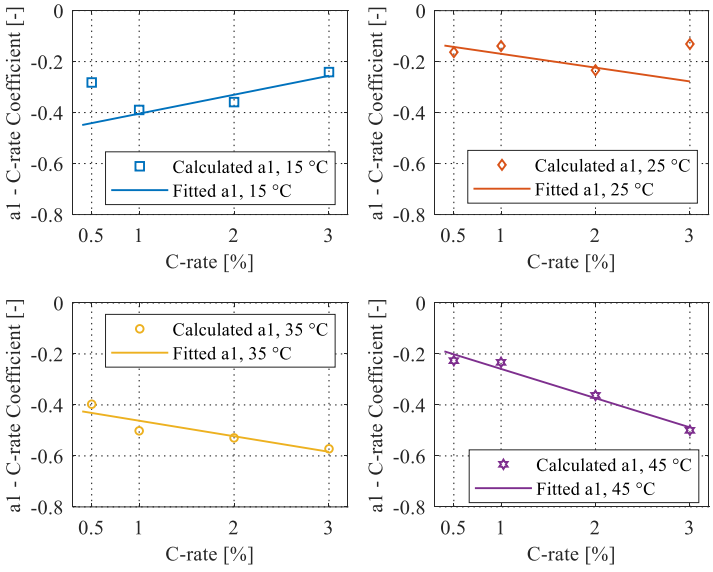

(a)

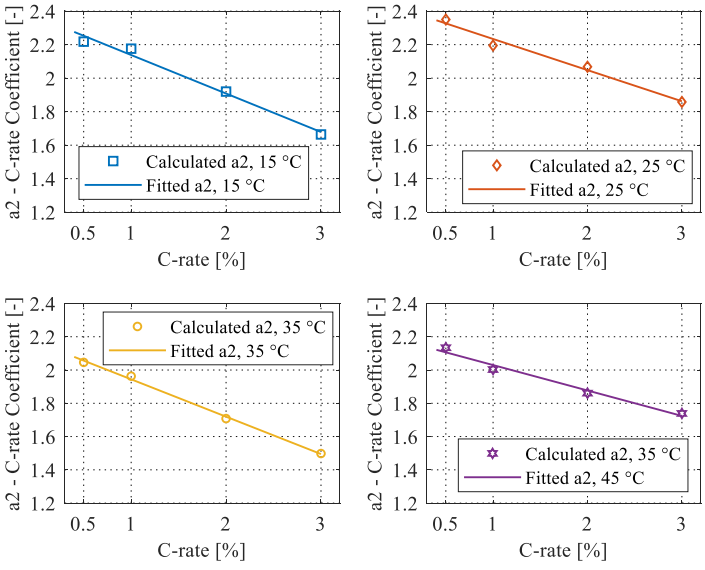

(b)

Fig. 3.12: (a) The relationship between the coefficient $A_1(C,T)$ and the current amplitude; (b) the relationship between the coefficient $A_2(C,T)$ and the current amplitude.

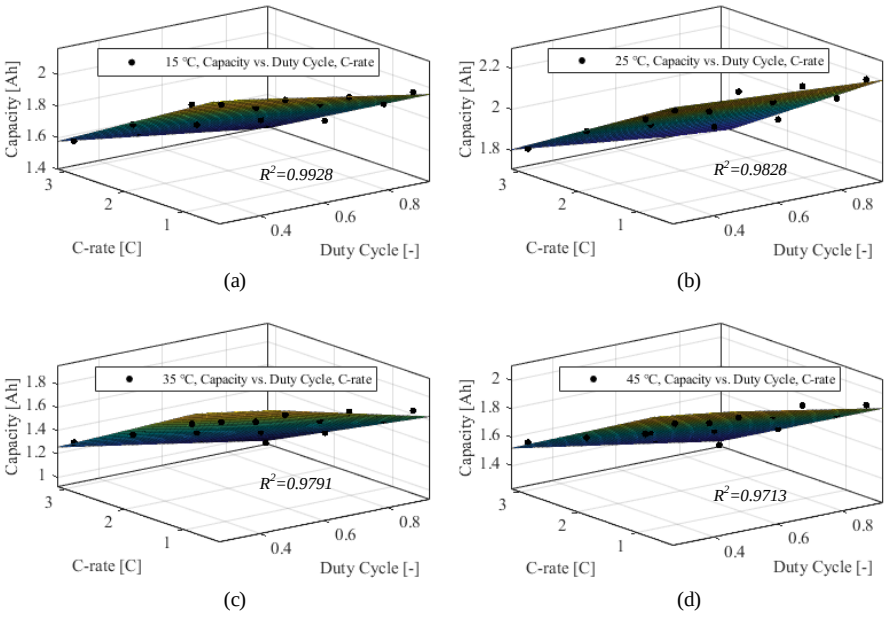

Fig. 3.13: Measured and the fitted capacity based on the proposed capacity model: (a)-(d) correspond to 15 °C, 25 °C, 35 °C, and 45 °C, respectively.

described in (3.16):

$$\begin{aligned}\begin{bmatrix} A_1(C,T) & A_2(C,T) \end{bmatrix} &= \begin{bmatrix} C & 1 \end{bmatrix} \cdot B_{2\times 2}(T) \\ &= \begin{bmatrix} C & 1 \end{bmatrix} \cdot \begin{bmatrix} B_{11}(T) & B_{21}(T) \\ B_{12}(T) & B_{22}(T) \end{bmatrix}\end{aligned} \tag{3.16}$$

where $B_{2\times 2}(T)$ is the temperature-dependent fitting coefficient of $A_{1\times 2}(C,T)$. The coefficient $B_{2\times 2}(T)$ at different temperatures is provided, as follows:

$$\begin{cases} B_{2\times 2}(T = 15\ ^\circ\text{C}) = \begin{bmatrix} 0.02562 & -0.2297 \\ -0.3594 & 2.368 \end{bmatrix} \\ B_{2\times 2}(T = 25\ ^\circ\text{C}) = \begin{bmatrix} -0.02704 & -0.1648 \\ -0.09992 & 2.368 \end{bmatrix} \\ B_{2\times 2}(T = 35\ ^\circ\text{C}) = \begin{bmatrix} 0.0722 & -0.3154 \\ -0.6929 & 2.368 \end{bmatrix} \\ B_{2\times 2}(T = 45\ ^\circ\text{C}) = \begin{bmatrix} 0.009368 & -0.2375 \\ -0.416 & 2.368 \end{bmatrix} \end{cases} \tag{3.17}$$

Then, the charging capacity considering various conditions, i.e., duty cycles, the cur-

rent rate of the amplitude, and ambient temperature, can be obtained:

$$Cap(D, C, T) = \begin{bmatrix} C & 1 \end{bmatrix} \cdot B_{2\times 2}(T) \cdot \begin{bmatrix} D \\ 1 \end{bmatrix} \tag{3.18}$$

Fig. 3.13 presents the battery capacity. The marked points are the measured value of the capacity. The colored surface is the capacity obtained by the proposed model.

The relationship between the temperature-dependent coefficient and the capacity should be further explored. However, the temperature-dependent coefficient could not achieve with high accuracy. This might result from the fact that the cell used in this work has a cycle life of 800 cycles, according to the datasheet. The battery cell was performed approximately 20 cycles at each ambient temperature condition. Even though it could be roughly assumed that the battery capacity is not significantly degraded, at least 80 cycles were performed on the tested battery cell; this could affect the cell's capacity.

5) Pulsed charging time modeling

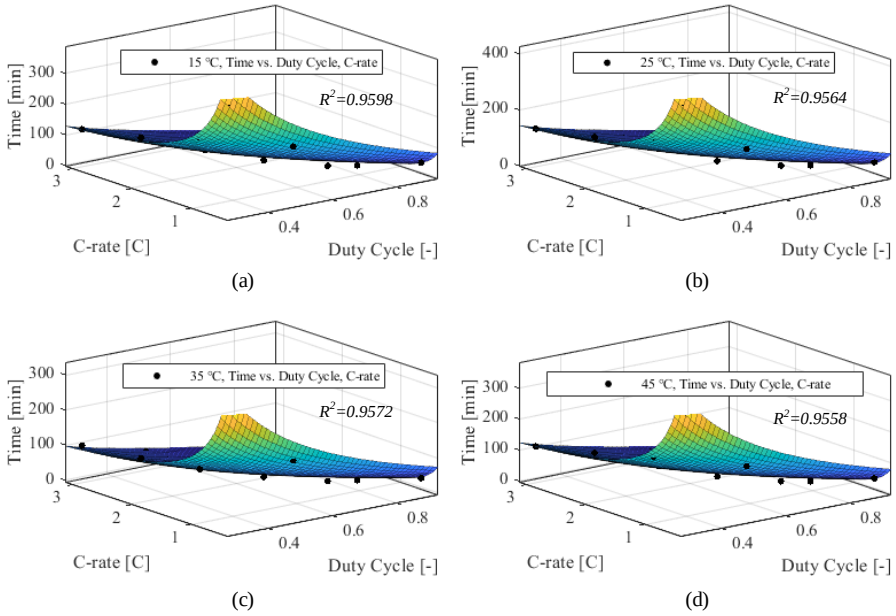

Fig. 3.14: Measured and fitted charging time based on the proposed model: (a)-(d) correspond to 15 °C, 25 °C, 35 °C, and 45 °C, respectively.

The charging time can be parameterized as the way of the capacity modeling. Fig. 3.14 shows the charging time under various conditions (see marked points in Fig. 3.14). A function has been explored to fit the charging time obtained by different test conditions, as the colored surface shown in Fig. 3.14. The charging time of the PPC

can be expressed, as follows:

$$t(D,C,T) = 60 \cdot N_{1\times3}(T) \cdot \begin{bmatrix} \frac{1}{D\cdot C} \\ -3\cdot D \\ 2 \end{bmatrix} \tag{3.19}$$

where $N_{1\times3}(T)$ is the temperature-dependent coefficient. The coefficient $N_{1\times3}(T)$ at different ambient temperatures is given, as follows:

$$\begin{cases} N_{1\times3}(T = 15\ ^\circ C) = \begin{bmatrix} 0.6705 & 0.9678 & 1.0642 \end{bmatrix} \\ N_{1\times3}(T = 25\ ^\circ C) = \begin{bmatrix} 0.7207 & 1.075 & 1.2067 \end{bmatrix} \\ N_{1\times3}(T = 35\ ^\circ C) = \begin{bmatrix} 0.5912 & 0.7039 & 0.7472 \end{bmatrix} \\ N_{1\times3}(T = 45\ ^\circ C) = \begin{bmatrix} 0.653 & 0.9317 & 1.0192 \end{bmatrix} \end{cases} \tag{3.20}$$

3.4.3 Discussion

This work mainly investigated the impacts of the parameters of the PPC mode on battery performance. According to the experimental results, the duty cycle and the current amplitude can significantly influence the battery performance. The battery charged by the PPC mode with a lower duty cycle can obtain a higher capacity and lower maximum rising temperature, while the charging time proportionally increases. This is because the duty cycle directly determines the average charging current. The current amplitude shows a similar impact on the charging performance as the duty cycles because the average charging current is also related to the current amplitude. However, the PPC mode with various duty cycles and amplitudes has no considerable improvement on the charging performances compared to the CC mode at the same average charging current level.

3.5 Summary

To investigate the effect of the pulsed current on the performance of lithium-ion batteries, various test conditions, i.e., current modes, frequency, duty cycle, current amplitude, and ambient temperature, were considered in this chapter. The investigated charging performance is battery capacity, charging time, maximum rising temperature. The pulsed current (i.ie., APC mode) can improve the obtained capacity by up to 6.2% when compared with the CC mode. Moreover, higher capacity of the battery cell can be obtained by the negative-pulse group (i.e., NPC mode, APC mode, and ASRC mode) than the positive-pulse group (i.e., PPC mode, PCCC mode, and SRC mode). However, the current mode in the negative-pulse group results in a higher maximum rising temperature due to the higher RMS value I_{rms} when compared with the CC mode and current modes in the positive-pulse group. The charging time/charging speed is directly determined by the average charging current instead of the current mode. The effects of the frequency on overall charging performances

are not considerable. The duty cycle and amplitude of the pulsed charging current can affect the charging performance by changing the average charging current. A high duty cycle and amplitude can reduce the charging time but results in a lower capacity and a higher rising temperature. Even though there is some difference in the results, the pulsed current with various profiles, frequencies, duty cycles, and amplitudes has no significant improvement in the charging performance compared with the CC mode.

Chapter 4

Lifetime Analysis with Pulsed Charging Current

This chapter investigates the effects of pulsed charging current on battery lifetime, considering a wide frequency range between 0.05 Hz and 2 kHz. The related outcomes are listed as follows:

J3. **X. Huang**, W. Liu, J. Meng, Y. Li, S. Jin, R. Teodorescu, and D. I. Stroe, "Lifetime Extension of Lithium-ion Batteries with Low-Frequency Pulsed Current Charging" *IEEE J. Emerg. Sel. Topics Power Electron.*, under review, 2021.

C2. **X. Huang**, S. Jin, J. Meng, R. Teodorescu, and D. I. Stroe, "The Effect of Pulsed Current on the Lifetime of Lithium-ion Batteries" in *Proc. IEEE ECCE*, accepted, 2021.

4.1 Introduction

The lifetime of Lithium-ion batteries is affected by the capacity and power fade during cycling. The degradation of lithium-ion batteries is mainly related to the loss of lithium inventory (LLI) and loss of active material (LAM) [17, 74]. The formation and growth of solid electrolyte interface (SEI) film are two of the important factors of the side reactions, which result in the LLI [75]. The decrease in power capability results from the increase in IR. Incremental capacity analysis (ICA) is one of methods for diagnosing the degradation of lithium-ion batteries [76]. The ICA curve shows the way of the capacity increment (dQ/dV) changing with battery voltage (V) [76, 77]. To obtain the ICA curve, it only needs to perform a charging/discharging cycle with a constant current on the batteries. Thus, the curve-based analysis is a practical method due to the advantages of non-destructivity and simple implementation [77]. In [78], the degradation of batteries has two stages by analyzing the evolution of ICA curves. During the first stage, the capacity fade of the battery is mainly caused by LLI. The LLI results from the parasitic reactions, which can form the SEI layer on the

electrode surfaces. The degradation caused by LLI continues during the second stage, following the same way as the first stage. At the same time, the degradation mode of LAM occurs, which results in the accelerated capacity fade of the battery cell [78]. Generally, the battery cell reaches its end of life (EOL) when it has a 20% capacity loss. Moreover, after this, the rate of the capacity fade will increase. However, the second stage of battery degradation occurs before the battery reaches its EOL. This means the degradation of the battery cell starts the second stage before occurring the accelerated capacity fade. Therefore, the degradation modes of the lithium-ion batteries can be analyzed by the degradation stage.

This chapter investigates the effects of PPC charging on the lifetime of lithium-ion batteries from three aspects, i.e., capacity fade, IR evolution, and the ICA curve. The experimental procedures are introduced in Section 4.2. Section 4.3 presents the experimental results. The degradation analysis is presented in Section 4.4. The summary is given in Section 4.5.

4.2 Experimental Method

The entire experiment test includes two parts, i.e., cycle aging test and reference performance test, as shown in Fig. 4.1. In the cycle aging test, there are six test cases with different charging conditions, i.e., CC, 0.05-Hz PPC, 0.2-Hz PPC, 1-Hz PPC, 100-Hz PPC, and 2-kHz PPC. The aging tests of the PPC charging at three low frequencies, i.e., 0.05 Hz, 0.2 Hz, and 1 Hz, were implemented on the Digatron battery test system, as shown in Fig. A.2 (see Appendix A.2). The aging tests of the PPC charging at two high frequencies, i.e., 100 Hz and 2 kHz, were performed using the Kepco bidirectional programmable power supply, as shown in Fig. A.1 (see Appendix A.1). All reference performance tests were performed using the Digatron battery test system.

The duty cycle and the amplitude of the PPC charging are 50% and 2 C, respectively. To maintain the average current, the amplitude of the CC charging is 1 C. For each cycle of the aging test, the battery was charged by the CC or PPC until the voltage reaches the maximum voltage V_{max}. Then, the battery was discharged by a 2-C constant current. To accelerate the degradation, all the aging tests were performed at 35 °C. Furthermore, 1000 cycles will be performed on the cells during all the aging tests. The temperature of the reference performance test is 25 °C for all tested batteries. The reference performance tests were performed before the aging test procedure started and performed after every 100 cycles. The reference performance tests are used to obtain the capacity fade, IR evolution, and ICA curves.

The capacity tests are performed for each tested battery cell to determine the capacity fade during the aging process. The battery cells are fully charged with a 1-C CC-CV pattern; after a 1-h relaxation, the cells are fully discharged with a 1-C current. The obtained discharging capacity is considered the capacity of the tested battery cell. Then, the capacity fade of each cell Q_{fade} with respect to the corresponding initial capacity can be obtained:

$$Q_{fade}[\%] = (1 - \frac{Cap_N}{Cap_{init.}}) \times 100\% \tag{4.1}$$

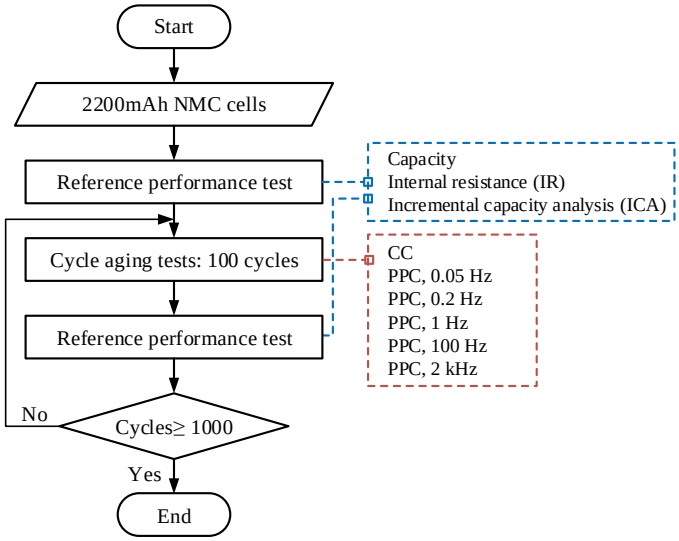

Fig. 4.1: Experimental procedures of the aging tests.

where N is the completed cycle number; Cap_N is the measured capacity after completing N cycles; $Cap_{init.}$ is the measured capacity before the cycle aging test.

The IR of the batteries was measured through the DC pulse technique [28, 79]. The test procedures for the IR measurement are the following:

1. Fully charge the battery cell using a 1-C CC-CV pattern until the maximum voltage of 4.2 V is reached.
2. Relax the battery cell 15 minutes at 25 °C.
3. Discharge the battery cell using a 1-C current to 90% SOC.
4. Relax the battery cell for 15 minutes at 25 °C.
5. Charge the battery cell using a 1-C current pulse for 18 seconds.
6. Relax the battery cell for 15 minutes at 25 °C.
7. Discharge the battery cell using a 1-C current pulse for 18 seconds.
8. Repete steps 2-7 for other SOCs: 70% 50%, 30%, and 10%.
9. Fully discharge the battery cell using a 1-C current until the minimum voltage of 2.5 V is reached.

Ohm's law is used to determine the IR of each battery:

$$IR = \frac{\Delta V_{18}}{I_{18}} \tag{4.2}$$

where ΔV_{18} is the voltage changes caused by the DC pulse I_{18}. The average of charging and discharging IRs was considered as the batteries' IR at the corresponding SOC.

The ICA method generally requires charging the battery with a very low current; for example, in [80], the authors use a 0.04 C rate. However, this will cost a very

long time for the measurement, which is not practical for real applications. The main behavior of the ICA curve can be observed when the charging/discharging current of the ICA curve is lower than 0.5 C [77]. Therefore, a 0.2-C CC is used to obtain the ICA curve. The sampling frequency is 1 Hz for all reference performance tests.

4.3 Experimental Results

4.3.1 Capacity Fade

Fig. 4.2 shows the capacity fade of the tested battery cells. After 500 cycles, the cell that was cycled by the CC charging reached its EOL, i.e., a 20% capacity fade. In contrast, the cells cycled by the PPC charging at the frequency range between 0.05 Hz and 100 Hz reached their EOL after 900 cycles, 900 cycles, 600 cycles, and 800 cycles, respectively. After 1000 cycles, the capacity fade of the cell caused by the CC charging is 62.16%, which is the largest one of all cases. It is followed by the battery cell using the 1-Hz PPC charging, presenting 42% capacity loss. The lowest capacity fade after 1000 cycles is 18.49%, which is from the cell that was cycled by 2-kHz PPC charging. This means the cell has not reached the EOL yet. Therefore, the PPC charging can slow down the degradation of lithium-ion battery cells in the considered frequency range. Moreover, the frequency can influence the effects of the PPC charging on the lifetime of the battery cells.

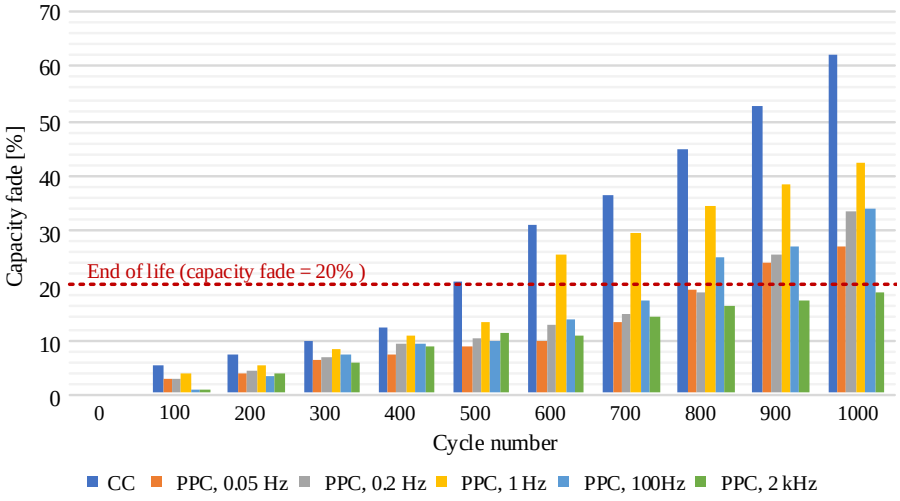

Fig. 4.2: Capacity fade of the tested battery cells during the aging tests.

4.3.2 Internal Resistance

Fig. 4.3 shows the evolution of the measured IR of the battery cell that was cycled by 0.05-Hz PPC. As expected, higher IR is obtained at low SOCs (i.e., 10%) than high SOCs (i.e., 30%-90%) The IR is quasi-independent on SOC between the range of 30% and 90%, independent of the cycle number. Thus, the IR at 50% SOC is considered to represent the IR of this SOC range.

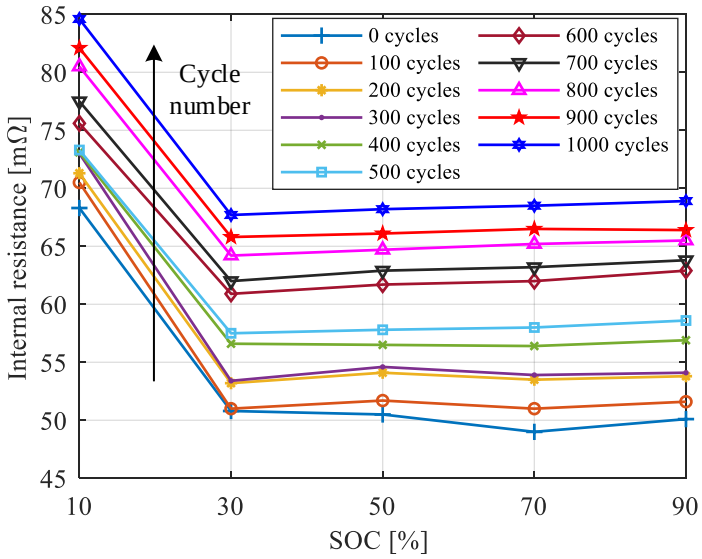

Fig. 4.3: Dependence of the IR on the SOC at different aging states, for the cell aged by 0.05 Hz PPC; the IR is the average value of the charging and discharging IRs, which were obtained at 25 °C with the 1-C 18-s charging and discharging current.

Figs. 4.4(a) and (b) show the percentage increases in IR at 10% SOC and 50% SOC. It can be observed that the IR evolution at 10% SOC is slower than that of 50% SOC for all cells. However, both of them show an increasing trend. The CC charging results in a much faster IR increase during the aging test than the PPC charging. For the PPC charging, the increase in the IR shows a parabolic profile with increasing frequency for both SOC conditions.

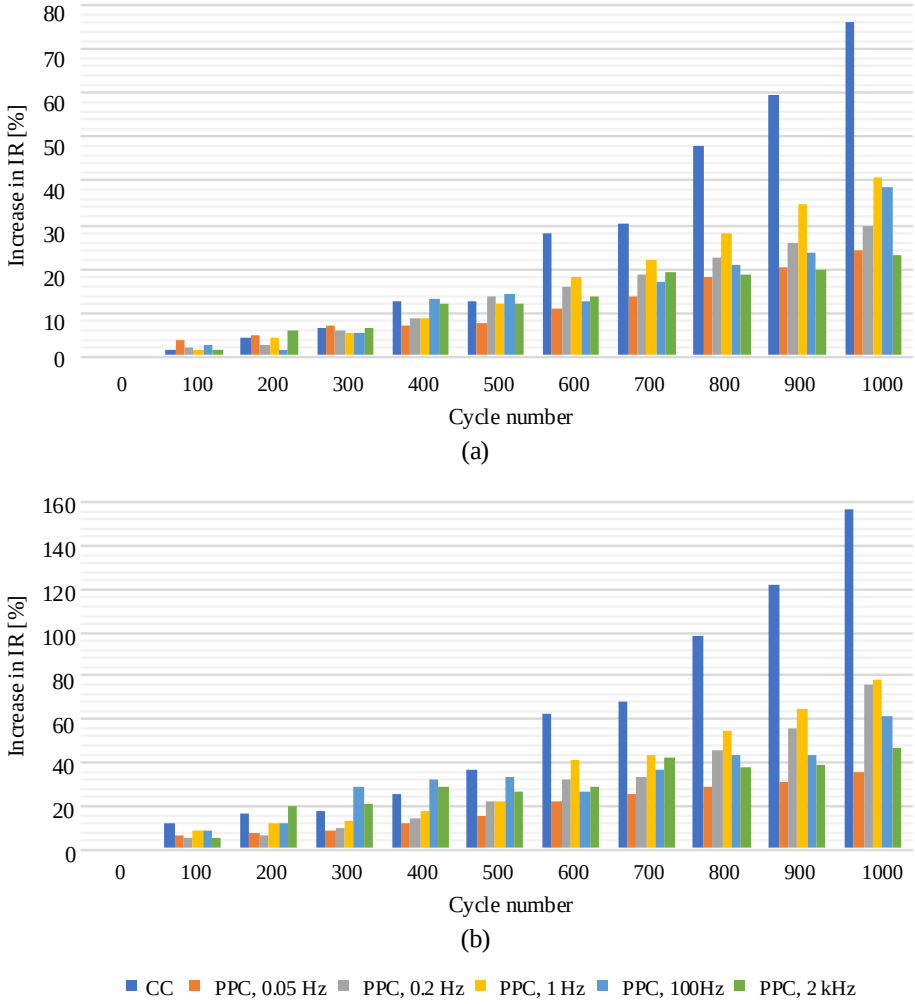

Fig. 4.4: Internal resistance (IR) evolution during the aging process: (a) SOC=10% and (b) SOC=50%.

4.3.3 Incremental Capacity Analysis

Fig. 4.5 shows the ICA curves at different aging states of the tested battery cells. In Fig. 4.5(a)-(e), the three curves in each figure presented are obtained when the battery cells were fresh, reached their EOL, and completed 1000 cycles. Fig. 4.5(f) shows the ICA curve of the PPC charging at 2 kHz. After 1000 cycles, the cell that was cycled by 2-kHz PPC has not reached its EOL; thus, there were only two ICA curves for this case. When battery cells were fresh, three ICA peaks, i.e., peak ①, peak ②, and peak ③, can be observed. The density of those peaks decreased with increasing cycle numbers. When the tested cells reached their EOL, the ICA values

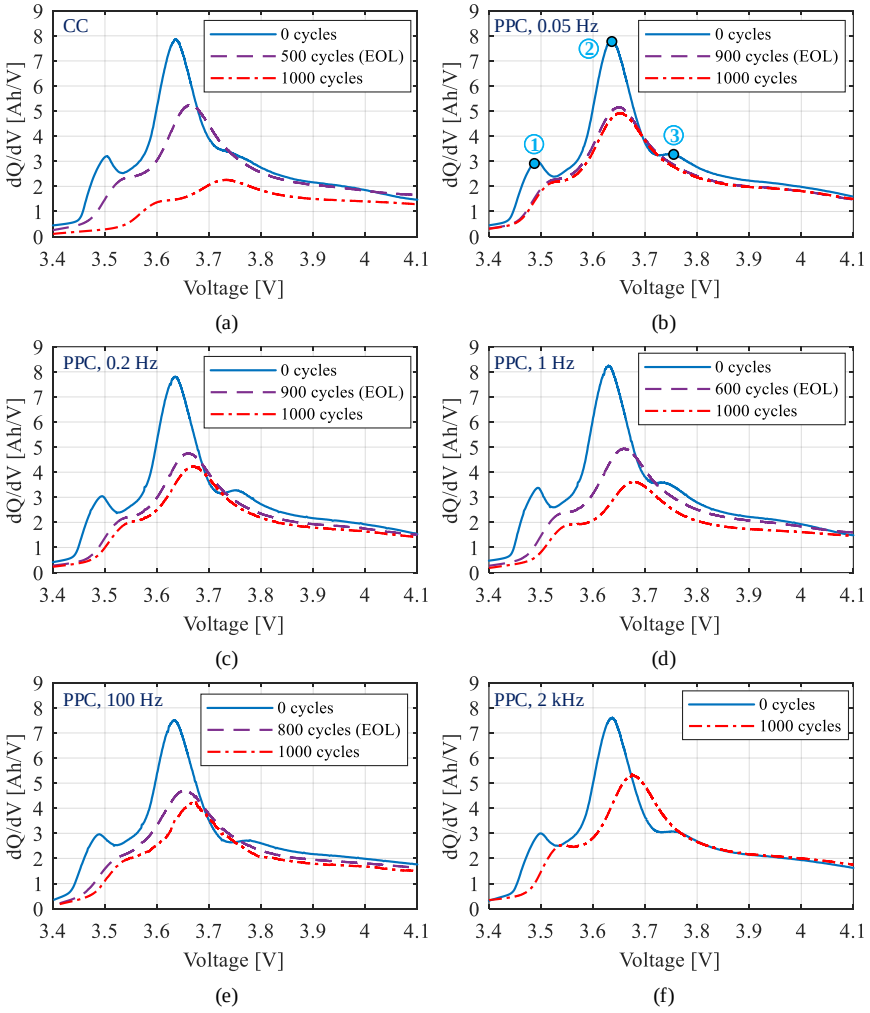

Fig. 4.5: Incremental Capacity Analysis (ICA) curves at BOL, EOL, and after 1000 cycles for the tested cells that were cycled with different charging currents: (a) CC, (b)-(g) PPC at 0.05 Hz, 0.2 Hz, 1 Hz, 100 Hz, and 2 kHz, respectively.

of peak ① are around 5 Ah/V. Except for the cases of 0.05-Hz and 2-kHz PPC, the ICA values of peak ① are significantly lower than 5 Ah/V after 1000 cycles. The ICA value of the CC-charging case at peak ① is around 2.3 Ah/V after 1000 cycles, which is lower than half of the ICA value of the 2-kHz PPC charging. The decrease in peak density is consistent with the degradation of the battery cells. Moreover, the position of peaks ① and peak ② move to a higher voltage compared to their initial positions with increasing cycle numbers. Furthermore, the peak ③ of all cases can not be observed after the entire cycling tests.

4.4 Degradation Analysis

In this section, a two-stage degradation model is developed to investigate the effect of the PPC and its frequency on the degradation of batteries. Based on the degradation model, the lifetime extension obtained by the PPC charging with different frequencies is obtained. The effects of the PPC charging on degradation modes are analyzed by combining the experimental results (i.e., capacity fade, IR evolution, and the ICA) and the degradation model.

4.4.1 Degradation Modeling

In Fig. 4.6, the marked points are the values of the measured capacity fade for each battery cell. Accelerated capacity fade can be observed at a specific cycle number, e.g., the 400th cycle of the CC charging and the 500th cycle of 1-Hz PPC charging. This means that before these cycle numbers, the corresponding battery cell has been entered aging stage 2, which is earlier than the occasion of the accelerated capacity fade. Therefore, the battery cell that was cycled by the CC charging entered stage 2 before the 400th cycle, i.e., around the 300th cycle. After 300 cycles, the capacity fade of the cell using the CC charging is 10%. Therefore, the capacity fade of 10% is regarded as the boundary of the change in the degradation mode, as shown in Fig. 4.6.

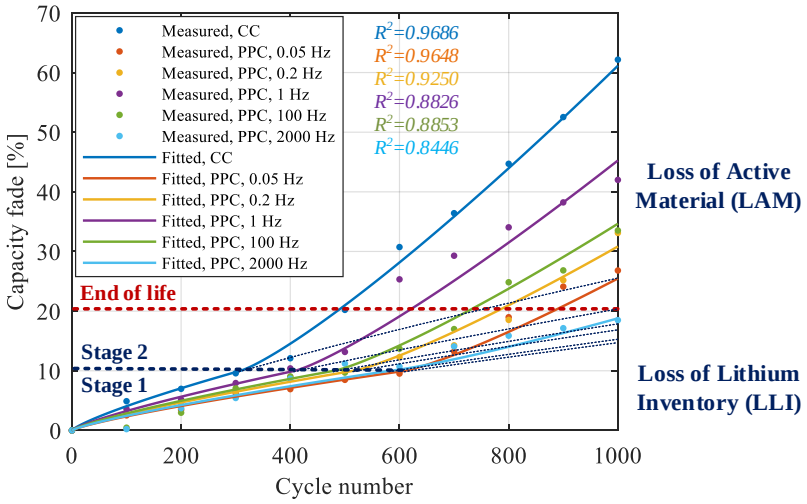

Fig. 4.6: Capacity fade of the tested cells that were cycled by the CC and PPC.

To investigate the effects of the PPC charging on the degradation of lithium-ion batteries at different aging stages, a two-stage degradation model is developed using a piecewise power function. The function was considered to fit the capacity fade as

follows:

$$\begin{cases} Q_{fade.s1}(N)[\%] = a_1 \cdot N^{0.8}, & when \quad Q_{fade} \leq 10\% \\ Q_{fade.s2}(N)[\%] = a_2 \cdot (N - N_{s1})^{1.2} + 10, & when \quad Q_{fade} > 10\% \end{cases} \tag{4.3}$$

where $Q_{fade.s1}$ and $Q_{fade.s2}$ are the capacity fade of the battery cell at stage 1 and stage 2, respectively; a_1 and a_2 are the fitting coefficient of stage 1 and stage 2; N_{s1} is the cycle number when the degradation of the cell reached to a 10% capacity fade. The value 10 at the second function is the initial value of stage 2, i.e., the 10% capacity fade.

The coefficients a_1 and a_2 describe the rate of the capacity fade for the tested battery cells. For the PPC charging, the relationship between the coefficient, i.e., $a_1(f)$ and $a_2(f)$, and the frequency were found and are given by:

$$a_1(f) = -3.554 \cdot 10^{-3} \cdot (log_{10}f)^2 + 7.035 \cdot 10^{-3} \cdot log_{10}f + 0.07533 \tag{4.4}$$

$$a_2(f) = -1.36 \cdot 10^{-3} \cdot (log_{10}f)^2 + 1.628 \cdot 10^{-3} \cdot log_{10}f + 0.01577 \tag{4.5}$$

Fig. 4.7 shows the dependence of the coefficient at stage 1 $a_1(f)$ and stage 2 $a_2(f)$ on the frequency of the PPC charging. It can be observed that the coefficients of both stage 1 and stage 2 at 1 Hz are higher than that of other frequencies. This means 1-Hz PPC charging shows the fastest capacity fade between all cases. Moreover, the frequencies at the two ends, i.e., 0.05 Hz and 2 kHz, show lower fitting coefficients when compared with the frequencies in the middle range. Thus, both the lower frequency and the higher frequency can further slow down the degradation of the batteries when compared to the middle frequency, such as 1 Hz.

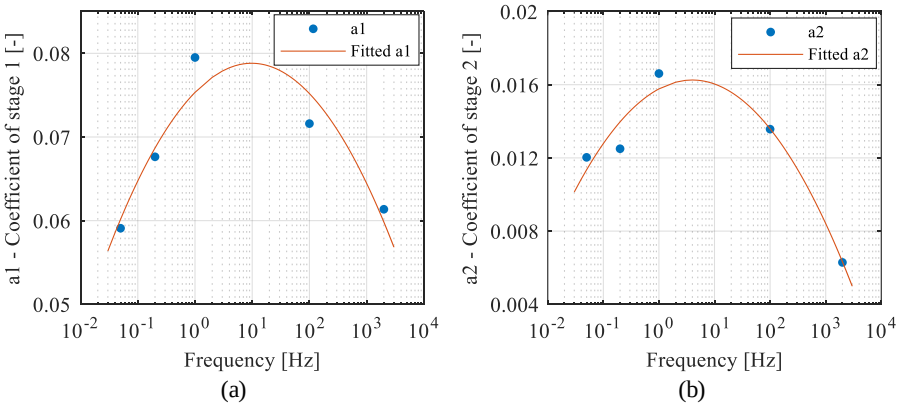

Fig. 4.7: Relationship between the frequency coefficient and frequency: (a) at stage 1 $a_1(f)$ and (b) at stage 2 $a_2(f)$.

The values of the fitting coefficients are provided in Table 4.1. The coefficients a_1 and a_2 of the CC charging are higher than that of PPC charging. Therefore, the PPC charging can extend the battery lifetime by slow down the degradation process of both stages.

Table 4.1: Fitting coefficient of the capacity fade for the tested battery cells.

Coefficient	CC	PPC				
		0.05 Hz	0.2 Hz	1 Hz	100 Hz	2000 Hz
a_1	0.10201	0.05909	0.06763	0.07951	0.07161	0.06136
a_2	0.01998	0.01203	0.01251	0.01661	0.01357	0.00629

Therefore, the degradation model of the PPC charging can be further expressed as the function that is related to the cycle number N and the frequency f, as follows:

$$\begin{cases} Q_{fade.s1}(f,N)[\%] = a_2(f)\cdot N^{0.8}, & when \quad Q_{fade} \leq 10\% \\ Q_{fade.s2}(f,N)[\%] = a_2(f)\cdot (N-N_{s1})^{1.2}+10, & when \quad Q_{fade} > 10\% \end{cases} \tag{4.6}$$

4.4.2 Lifetime extension

Based on the degradation model, the tested cell that was aged by the CC charging reached its EOL after 486 cycles; and the cells that were cycled by the PPC charging at the frequency range between 0.05 Hz and 2 kHz reached their EOL after 881 cycles, 779 cycles, 615 cycles, 725 cycles, 1048 cycles. Therefore, the PPC charging at the frequency range between 0.05 Hz and 2 kHz can extend the battery lifetime by 72.8%, 52.8%, 20.6%, 42.2%, and 105.5%, respectively. The lifetime extension of the PPC charging at different frequencies with respect to the standard lifetime achieved with the CC charging is presented in Fig. 4.8 (see the marked blue points).

The relationship between the percentage of lifetime extension $LTE(f)$ and the frequency f of the PPC charging can be expressed as a fuction and is give as follows:

$$LTE(f)[\%] = 13.36\cdot(log_{10}f)^2 - 19.85\cdot log_{10}f + 26.22 \tag{4.7}$$

The fitting result of the lifetime extension is shown in Fig. 4.8. Compared with CC charging, PPC charging can at least improve the battery lifetime by 18.9%. Taking 6 Hz, the frequency with the lowest lifetime extension, as the reference point, both increasing or decreasing the frequency of the PPC charging can further extend the battery lifetime.

4.4.3 Degradation Modes

In Fig. 4.5, the density of ICA peak ② is directly related to the capacity fade of the battery cells. Before the capacity fade reaches 10%, LLI is the main degradation mode that resulted in the capacity fade of the batteries. The LLI results from the parasitic reactions, which can form the SEI layer on the electrode surfaces. Therefore, the PPC can maintain the battery capacity by inhibiting SEI layer growth in stage 1. Moreover, this inhibitory effect can be further strengthened when the frequency of PPC charging is 0.05 Hz or 2 kHz. In Fig. 4.7, the fitting coefficients a_1 and a_2 can be used to compare the rate of the capacity fade resulted from the different charging currents.

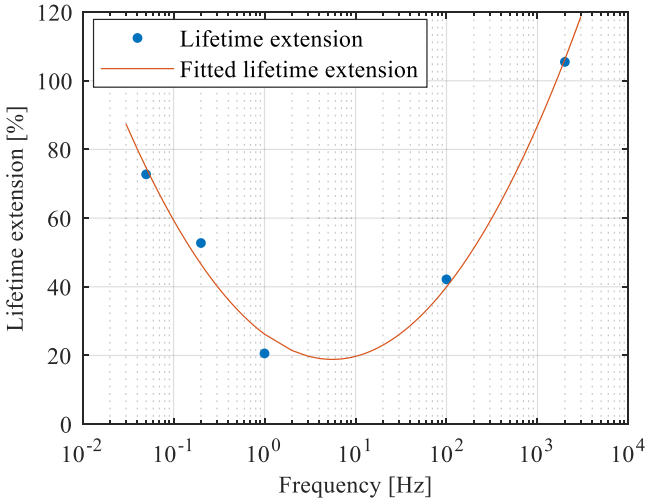

Fig. 4.8: Lifetime extension of the PPC charging at different frequencies when compared with the CC charging.

According to the value of a_1, both the pulsed charging current and frequency can influence the battery degradation process during stage 1, where 0.05-Hz PPC shows the lowest rate of the capacity fade. During stage 2, the degradation modes of LLI and LAM occurred together to accelerate the capacity loss of the tested battery cells. The capacity fade caused by LLI follows the same increased way as stage 1, i.e., the extension of each fitting curve shown in Fig. 4.6. The area between the extension line of the corresponding fitting curve at stage 1 and the x-axis is the capacity fade resulted from LLI. The area between the extension line and the corresponding fitting curve of stage 2 is the capacity degradation by LAM. The size of the area illustrates that the pulsed charging current not only has inhibiting effects on LLI but also can suppress the LAM. According to the value of coefficient a_2, the pulsed charging currents with different frequencies can inhibit the degradation of the second stage to varying degrees, where the 2-kHz PPC shows the best inhibiting effect. However, the degradation of stage 1 and stage 2 with the frequency shows a similar trend when compare the profile of the coefficients a_1 and a_2, as shown in Fig. 4.7.

The shift in the peak position of the ICA curve is another change with the aging process of the battery cells. The shift of the peak position is mainly caused by the increase in the IR of battery cells [71, 77, 78, 81]. The peak shift results in a decrease in the effective charging process, which means the battery is under discharging (UC) when the cell voltage reached the maximum voltage. The UC can be solved by setting a higher charging cut-off voltage [81]. However, the maximum charging voltage is a constant value in real applications. Moreover, how to reset a reasonable cut-off voltage is another issue that is needed to be explored. In Fig. 4.5, the broadening of the peaks can be observed, especially for the peak at low voltage position, i.e., peak ①. This mainly resulted from the SEI destabilization and disorder of graphite surface

during the aging process of the battery cells [74, 82]. Furthermore, the evolution of the IR prevents the phase transitions from occurring at the previous voltage position, thereby resulting in the disappearance of peak ③ [76].

4.5 Summary

This section investigated the effects of the PPC charging on the lifetime of lithium-ion battery cells which considers the frequency range between 0.05 Hz and 2 kHz. The effect of PPC charging on the battery lifetime is evaluated through the capacity fade, IR evolution, and ICA curve. The results indicate that the PPC charging can slow down the degradation of lithium-ion battery cells, and different frequencies will lead to the lifetime extension with different degrees. The IR degradation and ICA curve evolution show consistent with the capacity degradation. By developing a two-stage degradation model, the inhibiting effects of the PPC charging at different degradation stages were determined and analyzed. According to the value of the related model coefficient, the PPC charging can slow down the capacity fade by inhibiting the degradation process, i.e., LLI and LAM. The PPC charging at 2 kHz has the strongest suppression effect on the battery degradation. Based on the experimental results and the degradation model, the PPC charging at the frequency from 0.05 Hz to 2 kHz can extend the battery lifetime by 72.8%, 52.8%, 20.6%, 42.2%, and 105.5%, respectively, when compared with the CC charging. By modeling the lifetime extension compared to the CC charging, the PPC charging at 6 Hz can improve the battery lifetime by 18.9%, which is the lowest value of the lifetime extension. Taking 6 Hz as the reference point, both increasing or decreasing the frequency of the PPC charging can further extend the lifetime of lithium-ion batteries. Finally, the PPC charging at 2 kHz has the best performance in lifetime extension within the considered frequency range.

Chapter 5

Conclusions and Future Work

This chapter summarized the research work and contributions of the Ph.D. project - *The Effects of Pulsed Charging Current on Performance and Lifetime for Lithium-Ion Batteries*. The main outcomes and contributions are highlighted. The future research perspectives are provided in the end.

5.1 Conclusions

The main objective of this project was to prove the pulsed charging current can improve the performance and extend the lifetime of lithium-ion batteries. The project focused on the effects of the pulsed current charging under various test conditions on the performance and lifetime of lithium-ion batteries. Three technical objectives were considered in this thesis, and their results are summarized as follows.

The first technical objective was to review the pulsed current charging techniques. *Chapter 2* reviewed and defined various pulsed current modes. The effects of the positive current mode and negative pulsed current mode on the performance and lifetime of lithium-ion batteries were summarized, respectively. Then, the main factors that impact the charging speed, charging/discharging capacity, rising temperature, and lifetime, are analyzed and discussed according to the previous work. According to the current profile, five fundamental pulsed current modes were summarized, i.e., PPC mode, PCCC mode, NPC mode, APC mode, and SRC mode. The previous works mostly focused on the frequency and its effects on the performance and lifetime, while other parameters of the pulsed current, such as duty cycle and amplitude, were rarely mentioned.

The second technical objective was to investigate the effects of the pulsed charging current on the performance of lithium-ion batteries. In *Chapter 3*, various conditions of the pulsed charging current were considered, including the pulsed current mode, frequency, duty cycle, and amplitude. Different ambient temperatures were also considered in this work. The experimental results indicate that the pulsed current has no significant improvement in the overall charging performance when compared with the CC charging at the same average current level. Therefore, it can not be proved

that the pulsed charging current can improve the performance of lithium-ion batteries.

In *Chapter 4*, the last technical objective, i.e., the effects of pulsed charging current on the lifetime of lithium-ion batteries, was studied through experiments. By developing a two-stage degradation model, the pulsed current has inhibiting effects on the main degradation modes, i.e., LLI and LAM, thereby slowing down the capacity fade of batteries. Based on the experimental results and the degradation model, the PPC charging at frequencies from 0.05 Hz to 2 kHz can extend the lifetime by 72.8%, 52.8%, 20.6%, 42.2%, and 105.5%, respectively, when compared with the CC charging. By developing the lifetime extension model, the PPC charging can improve the battery lifetime by at least 18.9%. Finally, the PPC charging at 2 kHz has the best performance in lifetime extension within the considered frequency range.

Based on the above summary of this work, the main conclusions can be drawn:

- The pulsed current has no obvious advantages in improving the overall charging performances compared to the CC charging.
- The pulsed current can significantly extend the battery lifetime by more than 100% compared to the CC charging.

Therefore, the pulsed charging current is a promising charging strategy for future EVs due to its outstanding advantage in the lifetime extension of lithium-ion batteries.

5.2 Main Contributions

The main contributions achieved by this Ph.D. project can be summarized as follows:

- **An overview of the pulsed charging current for lithium-ion batteries**
  This thesis reviewed various pulsed current charging strategies. The fundamental pulsed current modes, i.e., PPC mode, PCCC mode, NPC mode, APC mode, and SRC mode, were summarized and defined in detail. Moreover, the effects of those current modes on the battery perfromance and lifetime were reviewed. Finally, the main factor that impacts the performance and lifetime was discussed by analyzing relevant literature.
- **The overall charging performance of lithium-ion batteries is not significantly affected by the pulsed current mode and its frequency**
  To investigate the effects of the pulsed current on battery performance, various tests conditions were considered, i.e., current mode, frequency, duty cycle, amplitude, and ambient temperature of the current pulse. Even though some differences resulting from various current modes and frequencies can be observed, the pulsed current has no obvious advantages in improving the investigated charging performances. The duty cycle and amplitude determine the average charging current, which is directly related to the charging performance. Overall, the performance of the lithium-ion batteries is not affected by the pulsed current mode, frequency, and other related parameters when compared with the CC mode with the same average current.

- **The lifetime of the lithium-ion batteries can be significantly extended by more than 100% using the pulsed current considering the suitable frequency**

  This thesis is the first work that experimentally investigated the effects of the pulsed current considering both the high frequencies and low frequencies on the battery lifetime. The investigated frequency range is between 0.05 Hz and 2 kHz. The results show that the PPC charging at different frequencies can improve battery lifetime to varying degrees. Moreover, the PPC charging at 2 kHz can extend the battery lifetime up to 105.5% when compared with the CC charging. Therefore, frequency is one of the critical factors that can influence the battery lifetime.

5.3 Future Research Perspectives

Although this Ph.D. has investigated some issues on the effects of the pulsed current charging on performance and lifetime of lithium-ion batteries, more challenges remain to be addressed in the future:

- **The effects of other parameters of the pulsed current on the lifetime of lithium-ion batteries.**

  This project studied the effects of PPC charging with different frequencies on the lifetime of lithium-ion batteries. However, the duty cycle and amplitude are the other two important parameters that can impact the PPC charging process and influence the battery lifetime. Thus, different duty cycles and amplitudes of the pulsed current should be considered in future investigations. Moreover, the ambient temperature can affect battery lifetime and should be considered in the next investigation.

- **The effects of the pulsed charging current on the lifetime of LFP-based batteries.**

  All experimental tests were performed using NMC-based battery cells. However, LFP-based batteries are expected to be widely applied in EV applications, especially in China. Thus, it is necessary to study the effects of the pulsed charging current on LFP-based batteries' lifetime.

- **The impacts of the pulsed charging current on the performance and lifetime of lithium-ion battery packs.**

  This work focused on the effects of the pulsed charging current on the single battery cell. However, lithium-ion batteries generally appear in the form of battery packs instead of battery cells in applications. Moreover, the pulsed current charging results in a higher cell temperature compared to the traditional CC charging. A slightly rising temperature for the battery cell will be a big challenge for battery packs, which are assembled by hundreds or even thousands of battery cells. Therefore, it is necessary to evaluate the impacts of the pulsed current charging on lithium-ion battery packs.

Bibliography

References

[1] P. Agreement, "Paris agreement," in *Report of the Conference of the Parties to the United Nations Framework Convention on Climate Change (21st Session, 2015: Paris). Retrived December*, vol. 4. HeinOnline, 2015, p. 2017.

[2] Q. Zhang, H. Li, L. Zhu, P. E. Campana, H. Lu, F. Wallin, and Q. Sun, "Factors influencing the economics of public charging infrastructures for EV – a review," *Renew. Sustain. Energy Rev.*, vol. 94, pp. 500–509, Oct. 2018.

[3] N. O. Kapustin and D. A. Grushevenko, "Long-term electric vehicles outlook and their potential impact on electric grid," *Energy Pol.*, vol. 137, p. 111103, Feb. 2020.

[4] IEA, "Global electric passenger car stock, 2010-2020," IEA, Paris, Tech. Rep., Apr. 2021.

[5] T. S. Ferreira, F. C. Trindade, Y. G. Pinto, and W. Freitas, "New analytical method for analysing the effectiveness of infrastructure reinforcement in electric power distribution systems," *Electr. Power Syst. Res.*, vol. 182, p. 106250, May 2020.

[6] IEA, "Electric vehicle stock in the ev30@30 scenario, 2018-2030," IEA, Paris, Tech. Rep., Jan. 2020.

[7] A. Farjah, T. Ghanbari, and A. R. Seifi, "Contribution management of lead-acid battery, li-ion battery, and supercapacitor to handle different functions in EVs," *Int. Trans. Electr. Energy Syst.*, vol. 30, no. 1, Jul. 2019.

[8] T. Mesbahi, A. Ouari, T. Ghennam, E. M. Berkouk, N. Rizoug, N. Mesbahi, and M. Meradji, "A stand-alone wind power supply with a li-ion battery energy storage system," *Renew. Sustain. Energy Rev.*, vol. 40, pp. 204–213, Dec. 2014.

[9] P. Ruetschi, "Aging mechanisms and service life of lead–acid batteries," *J. Power Sources*, vol. 127, no. 1-2, pp. 33–44, Mar. 2004.

[10] J. Viera, M. Gonzalez, J. Anton, J. Campo, F. Ferrero, and M. Valledor, "NiMH vs NiCd batteries under high charging rates," in *Proc. IEEE INTELEC*, Sep. 2006.

[11] Q. Lin, J. Wang, R. Xiong, W. Shen, and H. He, "Towards a smarter battery management system: A critical review on optimal charging methods of lithium ion batteries," *Energy*, vol. 183, pp. 220–234, Sep. 2019.

[12] S. McCluer and C. Jean-Francois, "White paper no. 65 rev.2 comparing data center batteries flywheels and ultracapacitors," Schneider Electric Data Center Sci. Center., Tech. Rep., 2011.

[13] N. Wang, L. Tang, and H. Pan, "Analysis of public acceptance of electric vehicles: An empirical study in shanghai," *Technol. Forecast. Soc. Chang.*, vol. 126, pp. 284–291, Jan. 2018.

[14] P. K. Nayak, L. Yang, W. Brehm, and P. Adelhelm, "From lithium-ion to sodium-ion batteries: Advantages, challenges, and surprises," *Angew. Chem. Int. Ed.*, vol. 57, no. 1, pp. 102–120, Nov. 2017.

[15] F. Duffner, L. Mauler, M. Wentker, J. Leker, and M. Winter, "Large-scale automotive battery cell manufacturing: Analyzing strategic and operational effects on manufacturing costs," *Int. J. Prod. Econ.*, vol. 232, p. 107982, Feb. 2021.

[16] J. Neubauer and A. Pesaran, "The ability of battery second use strategies to impact plug-in electric vehicle prices and serve utility energy storage applications," *J. Power Sources*, vol. 196, no. 23, pp. 10 351–10 358, Dec. 2011.

[17] C. R. Birkl, M. R. Roberts, E. McTurk, P. G. Bruce, and D. A. Howey, "Degradation diagnostics for lithium ion cells," *J. Power Sources*, vol. 341, pp. 373–386, Feb. 2017.

[18] J. Zhu, Z. Sun, X. Wei, H. Dai, and W. Gu, "Experimental investigations of an AC pulse heating method for vehicular high power lithium-ion batteries at subzero temperatures," *J. Power Sources*, vol. 367, pp. 145–157, Nov. 2017.

[19] T. M. Bandhauer, S. Garimella, and T. F. Fuller, "A critical review of thermal issues in lithium-ion batteries," *J. Electrochem. Soc.*, vol. 158, no. 3, p. R1, 2011.

[20] A. Cordoba-Arenas, S. Onori, Y. Guezennec, and G. Rizzoni, "Capacity and power fade cycle-life model for plug-in hybrid electric vehicle lithium-ion battery cells containing blended spinel and layered-oxide positive electrodes," *J. Power Sources*, vol. 278, pp. 473–483, Mar. 2015.

[21] L. Lander, E. Kallitsis, A. Hales, J. S. Edge, A. Korre, and G. Offer, "Cost and carbon footprint reduction of electric vehicle lithium-ion batteries through efficient thermal management," *Appl. Energy*, vol. 289, p. 116737, May 2021.

[22] X. Huang, X. Sui, D.-I. Stroe, and R. Teodorescu, "A review of management architectures and balancing strategies in smart batteries," in *Proc. IEEE IECON*, Oct. 2019.

[23] M. Hoque, M. Hannan, A. Mohamed, and A. Ayob, "Battery charge equalization controller in electric vehicle applications: A review," *Renew. Sustain. Energy Rev.*, vol. 75, pp. 1363–1385, Aug. 2017.

[24] Y. Li and Y. Han, "A module-integrated distributed battery energy storage and management system," *IEEE Trans. Power Electron.*, pp. 1–1, 2016.

[25] Y. Chen, X. Liu, Y. Cui, J. Zou, and S. Yang, "A multi-winding transformer cell-to-cell active equalization method for lithium-ion batteries with reduced number of driving circuits," *IEEE Trans. Power Electron.*, pp. 1–1, 2015.

[26] X. Huang, A. B. Acharya, J. Meng, X. Sui, D.-I. Stroe, and R. Teodorescu, "Wireless smart battery management system for electric vehicles," in *Proc. IEEE ECCE*, Oct. 2020.

[27] S. K. Rechkemmer, X. Zang, W. Zhang, and O. Sawodny, "Lifetime optimized charging strategy of li-ion cells based on daily driving cycle of electric two-wheelers," *Appl. Energy*, vol. 251, p. 113415, Oct. 2019.

[28] D.-I. Stroe, "Lifetime models for lithium ion batteries used in virtual power plants," in *Department of Energy Technology*. Aalborg University, 2014.

[29] H. Liu, I. H. Naqvi, F. Li, C. Liu, N. Shafiei, Y. Li, and M. Pecht, "An analytical model for the CC-CV charge of li-ion batteries with application to degradation analysis," *J. Energy Storage*, vol. 29, p. 101342, Jun. 2020.

[30] S. Y. Cho, I. O. Lee, J. I. Baek, and G. W. Moon, "Battery impedance analysis considering DC component in sinusoidal ripple-current charging," *IEEE Trans. Ind. Electron.*, vol. 63, no. 3, pp. 1561–1573, Mar. 2016.

[31] A. S. Mussa, M. Klett, M. Behm, G. Lindbergh, and R. W. Lindströßm, "Fast-charging to a partial state of charge in lithium-ion batteries: A comparative ageing study," *J. Energy Storage*, vol. 13, pp. 325–333, Oct. 2017.

[32] M. Xu, R. Wang, B. Reichman, and X. Wang, "Modeling the effect of two-stage fast charging protocol on thermal behavior and charging energy efficiency of lithium-ion batteries," *J. Energy Storage*, vol. 20, pp. 298–309, Dec. 2018.

[33] C.-H. Lee, M.-Y. Chen, S.-H. Hsu, and J.-A. Jiang, "Implementation of an SOC-based four-stage constant current charger for li-ion batteries," *J. Energy Storage*, vol. 18, pp. 528–537, Aug. 2018.

[34] L. Jiang, Y. Li, Y. Huang, J. Yu, X. Qiao, Y. Wang, C. Huang, and Y. Cao, "Optimization of multi-stage constant current charging pattern based on taguchi method for li-ion battery," *Appl. Energy*, vol. 259, p. 114148, Feb. 2020.

[35] H. A. Serhan and E. M. Ahmed, "Effect of the different charging techniques on battery life-time: Review," in *Proc. IEEE ITCE*, Feb. 2018.

[36] C. Praisuwanna and S. Khomfoi, "A pulse frequency technique for a quick charger," in *Proc. IEEE ECTI-CON*, May 2013.

[37] X. D. G. Gumera, A. B. Caberos, S.-C. Huang, W.-R. Liou, and J.-C. Lin, "A variable duty cycle pulse train charger for improving lead-acid battery performance," in *Proc. IEEE ACEPT*, Oct. 2017.

[38] Y. Chu, R. Chen, T. Liang, S. Changchien, and J. Chen, "Positive/negative pulse battery charger with energy feedback and power factor correction," in *Proc. IEEE APEC*.

[39] J. Li, E. Murphy, J. Winnick, and P. A. Kohl, "The effects of pulse charging on cycling characteristics of commercial lithium-ion batteries," *J. Power Sources*, vol. 102, no. 1-2, pp. 302–309, Dec. 2001.

[40] M. A. Monem, K. Trad, N. Omar, O. Hegazy, B. Mantels, G. Mulder, P. V. den Bossche, and J. V. Mierlo, "Lithium-ion batteries: Evaluation study of different charging methodologies based on aging process," *Appl. Energy*, vol. 152, pp. 143–155, Aug. 2015.

[41] J. A. Boadu, A. G. Elie, and E. S. Sinencio, "The impact of pulse charging parameters on the life cycle of lithium-ion polymer batteries," *Energies*, vol. 11, no. 8, p. 2162, Aug. 2018.

[42] D. R. R. Kannan and M. H. Weatherspoon, "The effect of pulse charging on commercial lithium nickel cobalt oxide (NMC) cathode lithium-ion batteries," *J. Power Sources*, vol. 479, p. 229085, Dec. 2020.

[43] P. Keil and A. Jossen, "Charging protocols for lithium-ion batteries and their impact on cycle life—an experimental study with different 18650 high-power cells," *J. Energy Storage*, vol. 6, pp. 125–141, May 2016.

[44] F. Savoye, P. Venet, M. Millet, and J. Groot, "Impact of periodic current pulses on li-ion battery performance," *IEEE Trans. Ind. Electron.*, vol. 59, no. 9, pp. 3481–3488, Sep. 2012.

[45] M. A. Monem, K. Trad, N. Omar, O. Hegazy, P. V. den Bossche, and J. V. Mierlo, "Influence analysis of static and dynamic fast-charging current profiles on ageing performance of commercial lithium-ion batteries," *Energy*, vol. 120, pp. 179–191, Feb. 2017.

[46] B. K. Purushothaman, P. W. Morrison, and U. Landau, "Reducing mass-transport limitations by application of special pulsed current modes," *J. Electrochem. Soc.*, vol. 152, no. 4, p. J33, 2005.

[47] H. J. Chiu, L. W. Lin, P. L. Pan, and M. H. Tseng, "A novel rapid charger for lead-acid batteries with energy recovery," *IEEE Trans. Power Electron.*, vol. 21, no. 3, pp. 640–647, May 2006.

[48] S. Zhu, C. Hu, Y. Xu, Y. Jin, and J. Shui, "Performance improvement of lithium-ion battery by pulse current," *J. Energy Chem.*, vol. 46, pp. 208–214, Jul. 2020.

[49] E. Schaltz, D.-I. Stroe, K. Norregaard, L. S. Ingvardsen, and A. Christensen, "Incremental capacity analysis applied on electric vehicles for battery state-of-health estimation," *IEEE Trans. Ind. Appl.*, vol. 57, no. 2, pp. 1810–1817, Mar. 2021.

[50] L.-R. Chen, "A design of an optimal battery pulse charge system by frequency-varied technique," *IEEE Trans. Ind. Electron.*, vol. 54, no. 1, pp. 398–405, Feb. 2007.

[51] L. R. Chen, "Design of duty-varied voltage pulse charger for improving li-ion battery-charging response," *IEEE Trans. Ind. Electron.*, vol. 56, no. 2, pp. 480–487, Feb. 2009.

[52] S. Sirisukprasert and S. I. Niroshana, "An adaptive pulse charging algorithm for lithium batteries," in *Proc. IEEE ECTI-CON*, Jun. 2017.

[53] S. M. I. Niroshana and S. Sirisukprasert, "Adaptive pulse charger for li-ion batteries," in *Proc. IEEE IC-ICTES*, May 2017.

[54] L. R. Chen, S. L. Wu, D. T. Shieh, and T. R. Chen, "Sinusoidal-ripple-current charging strategy and optimal charging frequency study for li-ion batteries," *IEEE Trans. Ind. Electron.*, vol. 60, no. 1, pp. 88–97, Jan. 2013.

[55] N. Majid, S. Hafiz, S. Arianto, R. Y. Yuono, E. T. Astuti, and B. Prihandoko, "Analysis of effective pulse current charging method for lithium ion battery," *J. Phys. Conf. Ser.*, vol. 817, p. 012008, Apr. 2017.

[56] Y. Saito, "Thermal behaviors of lithium-ion batteries during high-rate pulse cycling," *J. Power Sources*, vol. 146, no. 1-2, pp. 770–774, Aug. 2005.

[57] X. Huang, Y. Li, A. B. Acharya, X. Sui, J. Meng, R. Teodorescu, and D.-I. Stroe, "A review of pulsed current technique for lithium-ion batteries," *Energies*, vol. 13, no. 10, p. 2458, May 2020.

[58] Y. Zhao, B. Lu, Y. Song, and J. Zhang, "A modified pulse charging method for lithium-ion batteries by considering stress evolution, charging time and capacity utilization," *Front. Struct. Civil Eng.*, vol. 13, no. 2, pp. 294–302, Feb. 2018.

[59] Z. Jiang and R. Dougal, "Synergetic control of power converters for pulse current charging of advanced batteries from a fuel cell power source," *IEEE Trans. Power Electron.*, vol. 19, no. 4, pp. 1140–1150, Jul. 2004.

[60] N. Keskin and H. Liu, "Fast charging method for wireless and mobile devices using double-pulse charge technique," in *Proc. IEEE WPTC*, May 2014.

[61] B. K. Purushothaman and U. Landau, "Rapid charging of lithium-ion batteries using pulsed currents," *J. Electrochem. Soc.*, vol. 153, no. 3, p. A533, 2006.

[62] H. Fang, C. Depcik, and V. Lvovich, "Optimal pulse-modulated lithium-ion battery charging: Algorithms and simulation," *J. Energy Storage*, vol. 15, pp. 359–367, Feb. 2018.

[63] L. R. Chen, C. M. Young, N. Y. Chu, and C. S. Liu, "Phase-locked bidirectional converter with pulse charge function for 42-v/14-v dual-voltage PowerNet," *IEEE Trans. Ind. Electron.*, vol. 58, no. 5, pp. 2045–2048, May 2011.

[64] H. Lv, X. Huang, and Y. Liu, "Analysis on pulse charging–discharging strategies for improving capacity retention rates of lithium-ion batteries," *Ionics*, vol. 26, no. 4, pp. 1749–1770, Jan. 2020.

[65] T. Liang, T. Wen, K. Tseng, and J. Chen, "Implementation of a regenerative pulse charger using hybrid buck-boost converter," in *Proc. IEEE PEDS*.

[66] J. M. Amanor-Boadu and A. Guiseppi-Elie, "Improved performance of li-ion polymer batteries through improved pulse charging algorithm," *Appl. Sci.*, vol. 10, no. 3, p. 895, Jan. 2020.

[67] A. Bessman, R. Soares, S. Vadivelu, O. Wallmark, P. Svens, H. Ekstrom, and G. Lindbergh, "Challenging sinusoidal ripple-current charging of lithium-ion batteries," *IEEE Trans. Ind. Electron.*, vol. 65, no. 6, pp. 4750–4757, Jun. 2018.

[68] D. Ji, L. Chen, T. Ma, J. Wang, S. Liu, X. Ma, and F. Wang, "Research on adaptability of charging strategy for electric vehicle power battery," *J. Power Sources*, vol. 437, p. 226911, Oct. 2019.

[69] V. Knap, T. Zhang, D. I. Stroe, E. Schaltz, R. Teodorescu, and K. Propp, "Significance of the capacity recovery effect in pouch lithium-sulfur battery cells," *ECS Trans.*, vol. 74, no. 1, pp. 95–100, Dec. 2016.

[70] M. Uno and K. Tanaka, "Influence of high-frequency charge–discharge cycling induced by cell voltage equalizers on the life performance of lithium-ion cells," *IEEE Trans. Veh. Technol.*, vol. 60, no. 4, pp. 1505–1515, May 2011.

[71] A. Bessman, R. Soares, O. Wallmark, P. Svens, and G. Lindbergh, "Aging effects of AC harmonics on lithium-ion cells," *J. Energy Storage*, vol. 21, pp. 741–749, Feb. 2019.

[72] X. Huang, Y. Li, J. Meng, X. Sui, R. Teodorescu, and D.-I. Stroe, "The effect of pulsed current on the performance of lithium-ion batteries," in *Proc. IEEE ECCE*, Oct. 2020.

[73] K. Onda, T. Ohshima, M. Nakayama, K. Fukuda, and T. Araki, "Thermal behavior of small lithium-ion battery during rapid charge and discharge cycles," *J. Power Sources*, vol. 158, no. 1, pp. 535–542, Jul. 2006.

[74] M. Dubarry and B. Y. Liaw, "Identify capacity fading mechanism in a commercial LiFePO4 cell," *J. Power Sources*, vol. 194, no. 1, pp. 541–549, Oct. 2009.

[75] F. Yang, D. Wang, Y. Zhao, K.-L. Tsui, and S. J. Bae, "A study of the relationship between coulombic efficiency and capacity degradation of commercial lithium-ion batteries," *Energy*, vol. 145, pp. 486–495, Feb. 2018.

[76] R. Xiong, Y. Pan, W. Shen, H. Li, and F. Sun, "Lithium-ion battery aging mechanisms and diagnosis method for automotive applications: Recent advances and perspectives," *Renew. Sustain. Energy Rev.*, vol. 131, p. 110048, Oct. 2020.

[77] Y. Li, M. Abdel-Monem, R. Gopalakrishnan, M. Berecibar, E. Nanini-Maury, N. Omar, P. van den Bossche, and J. V. Mierlo, "A quick on-line state of health estimation method for li-ion battery with incremental capacity curves processed by gaussian filter," *J. Power Sources*, vol. 373, pp. 40–53, Jan. 2018.

[78] M. Dubarry, C. Truchot, B. Y. Liaw, K. Gering, S. Sazhin, D. Jamison, and C. Michelbacher, "Evaluation of commercial lithium-ion cells based on composite positive electrode for plug-in hybrid electric vehicle applications. part II. degradation mechanism under 2c cycle aging," *J. Power Sources*, vol. 196, no. 23, pp. 10 336–10 343, Dec. 2011.

[79] J. R. Belt, "Battery test manual for plug-in hybrid electric vehicles," Tech. Rep., Sep. 2010.

[80] M. Dubarry, C. Truchot, M. Cugnet, B. Y. Liaw, K. Gering, S. Sazhin, D. Jamison, and C. Michelbacher, "Evaluation of commercial lithium-ion cells based on composite positive electrode for plug-in hybrid electric vehicle applications. part i: Initial characterizations," *J. Power Sources*, vol. 196, no. 23, pp. 10 328–10 335, Dec. 2011.

[81] M. Dubarry, V. Svoboda, R. Hwu, and B. Y. Liaw, "Capacity and power fading mechanism identification from a commercial cell evaluation," *J. Power Sources*, vol. 165, no. 2, pp. 566–572, Mar. 2007.

[82] M. Dubarry, B. Y. Liaw, M.-S. Chen, S.-S. Chyan, K.-C. Han, W.-T. Sie, and S.-H. Wu, "Identifying battery aging mechanisms in large format li ion cells," *J. Power Sources*, vol. 196, no. 7, pp. 3420–3425, Apr. 2011.

Appendix A

Experimental Setup

A.1 Kepco Power Supply and NI Kit

Fig. A.1(a) presents the experimental setup, which includes a host computer, a National Instruments (NI) Data Acquisition (DAQ) module, and a Kepco bidirectional programmable power supply. The type number and the manufacturer of the related equipment are provided in Table A.1. In Fig. A.1(b), the battery test platform is developed by LabView to transfer the reference of the required current profiles to the power supply and log the measurement data of the battery voltage, current, and temperature. A VT 4002EMC climatic chamber is used to ensure a stable and reliable ambient temperature.

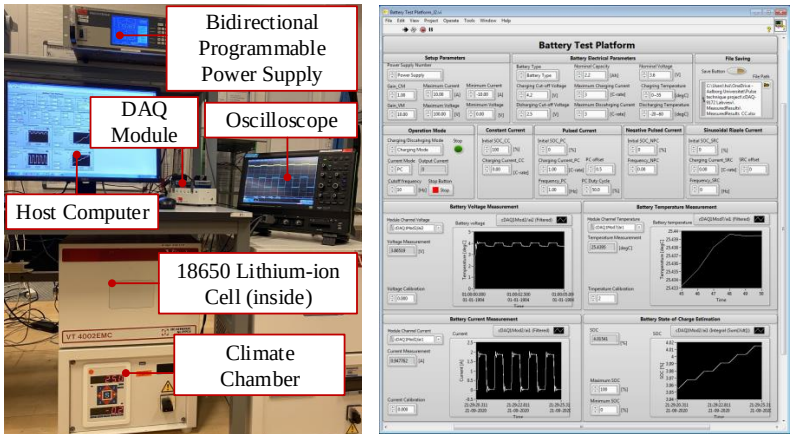

(a) (b)

Fig. A.1: Experimental setup based on a Kepco bidirectional programmable power supply (a) experimental setup and (b) user interface of the battery test platform.

Table A.1: Devices of the Experimental Setup.

Device	Number	Manufacturer
Bidirectional programmable power supply	BOP 100-10 MG	Kepco
Data acquisition module	cDAQ-9172	National Instruments
Analog output module	NI 9263	National Instruments
Analog input module	NI 9215	National Instruments
Thermocouple input module	NI 9211	National Instruments
Climatic chamber	VT 4002EMC	Vötsch Industrietechnik

A.2 Digatron Battery Test System

The Digatron battery test system is applied to perform the experiment and require and log the measured data. A Memmert temperature chamber is used to maintain a stable and reliable ambient temperature during the tests, as shown in Fig. A.2.

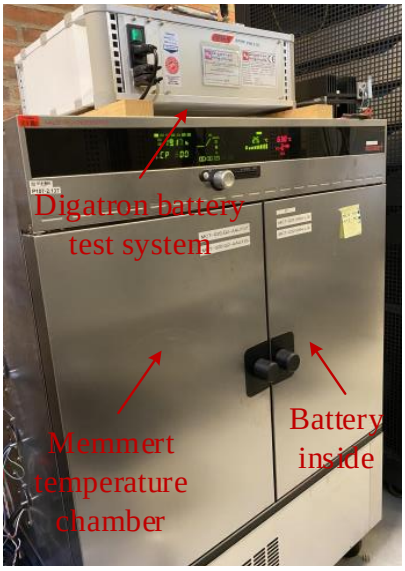

Fig. A.2: Experimental setup based on the Digatron battery test system.

Selected Publications

ISSN (online): 2446-1636
ISBN (online): 978-87-7210-080-7

AALBORG UNIVERSITY PRESS